NASA Contractor Report 3961

Analysis of Aerodynamic Coefficients Using Gust Gradient Data: Spanwise Turbulence Effects on Airplane Response

Erik A. Ringnes and Walter Frost

CONTRACT NAS8-35186
FEBRUARY 1986

NASA

NASA Contractor Report 3961

Analysis of Aerodynamic Coefficients Using Gust Gradient Data: Spanwise Turbulence Effects on Airplane Response

Erik A. Ringnes and Walter Frost
FWG Associates, Inc.
Tullahoma, Tennessee

Prepared for
George C. Marshall Space Flight Center
under Contract NAS8-35186

National Aeronautics
and Space Administration

**Scientific and Technical
Information Branch**

1986

ACKNOWLEDGMENTS

The work reported herein was supported by the National Aeronautics and Space Administration, Marshall Space Flight Center, Systems Dynamics Laboratory, Atmospheric Sciences Division, under Contract NAS8-35186.

The authors are indebted to Mr. A. Richard Tobiason of the Aerodynamic Division of the Office of Aeronautics and Space Technology, NASA Headquarters, Washington, D.C., for his support of this research. Special thanks are given to Mr. Dennis W. Camp, technical contract monitor for this study and to Mr. Harold Murrow for his effort in reviewing this report.

TABLE OF CONTENTS

LIST OF FIGURES

LIST OF SYMBOLS

A_n	Fourier series coefficients (dimensionless)
a	Wing lift curve slope (rad^{-1})
C_D	Drag coefficient (dimensionless)
C_{D_o}	Drag coefficient at zero angle of attack (dimensionless)
C_{D_α}	Drag derivative with respect to angle of attack (rad^{-1})
$C_{D_{\delta_r}}$	Drag derivative with respect to rudder deflection (rad^{-1})
$C_{D_{\delta_a}}$	Drag derivative with respect to aileron deflection (rad^{-1})
C_L	Lift coefficient (dimensionless)
C_{L_o}	Lift coefficient at zero angle of attack (dimensionless)
C_{L_q} .	Lift derivative with resepct to pitching rate (rad^{-1})
C_{L_α}	Lift derivative with respect to angle of attack (rad^{-1})
$C_{L_{\dot{\alpha}}}$	Lift derivative with respect to rate of change of angle of attack (rad^{-1})
$C_{L_{\delta_e}}$	Lift derivative with respect to elevator deflection (rad^{-1})
$C_{L_{i_t}}$	Lift derivative with respect to tail incidence angle (rad^{-1})
$C_L(y)$	Section lift coefficient
C_{ℓ_P}	Rolling moment derivative with respect to rolling rate (rad^{-1})

C_{ℓ_r}	Rolling moment derivative with respect to yawing rate (rad^{-1})
C_{ℓ_β}	Rolling moment derivative with respect to sideslip angle (rad^{-1})
$C_{\ell_{\delta_a}}$	Rolling moment derivative with respect to aileron deflection (rad^{-1})
$C_{\ell_{\delta_r}}$	Rolling moment derivative with respect to rudder deflection (rad^{-1})
C_m	Pitching moment coefficient (dimensionless)
C_{m_o}	Pitching moment coefficient at zero angle of attack (dimensionless)
C_{m_q}	Pitching moment derivative with respect to pitching rate (rad^{-1})
C_{m_α}	Pitching moment derivative with respect to angle of attack (rad^{-1})
$C_{m_{\dot{\alpha}}}$	Pitching moment derivative with respect to rate of change of angle of attack (rad^{-1})
$C_{m_{\delta_e}}$	Pitching moment derivative with respect to elevator deflection (rad^{-1})
C_{n_p}	Yawing moment derivative with respect to rolling rate (rad^{-1})
C_{n_r}	Yawing moment derivative with respect to yawing rate (rad^{-1})
C_{n_β}	Yawing moment derivative with respect to sideslip angle (rad^{-1})
$C_{n_{\delta_r}}$	Yawing moment derivative with respect to rudder deflection (rad^{-1})

$C_{n_{\delta_a}}$	Yawing moment derivative with respect to aileron deflection (rad^{-1})
C_{y_β}	Side force derivative with respect to sideslip angle (rad^{-1})
$C_{y_{\delta_r}}$	Side force derivative with respect to rudder deflection (rad^{-1})
c(y)	Section chord length (feet)
$\bar{c}$	Mean chord length (feet)
D	Drag force (lbf)
D_i	Induced drag force (lbf)
$d_i(y)$	Induced drag per unit span (lbf/feet)
F_y	Side force (lbf)
h	Normal distance from a vortex (m)
I_{nm}	Matrix with n rows and m columns
L	Lift force (lbf)
L	Rolling moment (ft-lbf)
L/W	Lift-to-weight ratio (dimensionless)
$\ell(y)$	Lift per unit span (lbf/ft)
$L_{SPANWISE}$	Lift force in a spanwise distributed wind (lbf)
$L_{UNIFORM}$	Lift force in a uniform wind field (lbf)
m	Mass of aircraft
M	Pitching moment (ft-lbf)
N	Yawing moment (ft-lbf)
P_{shape}	Shape factor (dimensionless)
P	Rolling rate (rad/sec)

q	Pitching rate (rad/sec)
r	Yawing rate (rad/sec)
s	Half-span length (ft)
t	Time (sec)
V_{avg}	Average airspeed (ft/sec)
V_c	Center probe airspeed (ft/sec)
V_L	Left probe airspeed (ft/sec)
V_R	Right probe airspeed (ft/sec)
$V(y)$	Airspeed (ft/sec)
v_i	Induced velocity (ft/sec)
$w(y)$	Downwash velocity (ft/sec)
x	x-axis in body coordinates (feet)
y	y-axis in body coordinates (feet)
z	z-axis in body coordinates (feet)

Greek Symbols

α	Angle of attack at aircraft center of gravity (rad)
$\alpha(y)$	Angle of attack at position y along the span (degrees)
α_{avg}	Average angle of attack (degrees)
α_c	Center probe angle of attack (degrees)
α_L	Left probe angle of attack (degrees)
α_R	Right probe angle of attack (degrees)

$\alpha_o(y)$	Zero lift angle (rad)
$\alpha_{eff}(y)$	Effective angle of attack (rad)
β	Sideslip angle (rad)
δ_a	Aileron deflection (rad^{-1})
δ_e	Elevator deflection (rad)
δ_r	Rudder deflection (rad)
$\delta\Gamma$	Strength of finitely small vortex filament
D_{ADD}	Drag due to spanwise turbulence (lbf)
L_{ADD}	Lift due to spanwise turbulence (lbf)
$\epsilon(y)$	Downwash angle at a position y along the span (rad)
$\Gamma(y)$	Circulation strength per unit span at a position y along the span
$\mu(y)$	Parameter defined by Equation 2.23 (rad^{-1})
θ	Pitching angle, positive nose up (rad)
ρ	Air density (lbm/ft^3)
ϕ	Rolling angle, positive right wing down (rad)
ψ	Yawing angle, positive nose right (rad)

Other

$(\dot{})$	Time derivative
$(\bar{})$	Time-averaged value

CHAPTER I

INTRODUCTION

Prediction of airplane response to atmospheric turbulence is commonly done with the assumption that the turbulence velocity varies along the flight path but does not vary along the span. In some previous studies where spanwise turbulence has been considered, power spectral methods were generally used (Coupry 1972, Fuller 1968). However, this investigation of the effects of spanwise turbulence is carried out in a different manner. Based on flight data, the aerodynamice forces and moments on the wing of NASA's B-57 aircraft are calculated using a modified vortex strip theory. This model allows the input airspeed and angle of attack to vary along the wing. Flight data provide three spatially separated records of the two input parameters. As a first order approximation, linear distributions in angle of attack and airspeed are assumed between the three recording locations; at the nose and at each wing tip (see Figure 1.1). For details on the B-57 instrumentation see Camp et al. (1984), Painter and Camp (1983), and Campbell et al. (1983). The modified vortex theory, hereafter referred to as the strip theory, has the ability to calculate lift and induced drag as a function of spanwise position. Furthermore, as in situations where these distributions are asymmetric, see Figure 1.2, an integration of these two forces over the wing span yields roll and yaw moments acting on the wing solely due to the asymmetric distribution of lift and drag. The results from strip theory calculations are next incorporated into a six-degrees-of-freedom (6DOF) program to investigate the effect of spanwise turbulence on aircraft response.

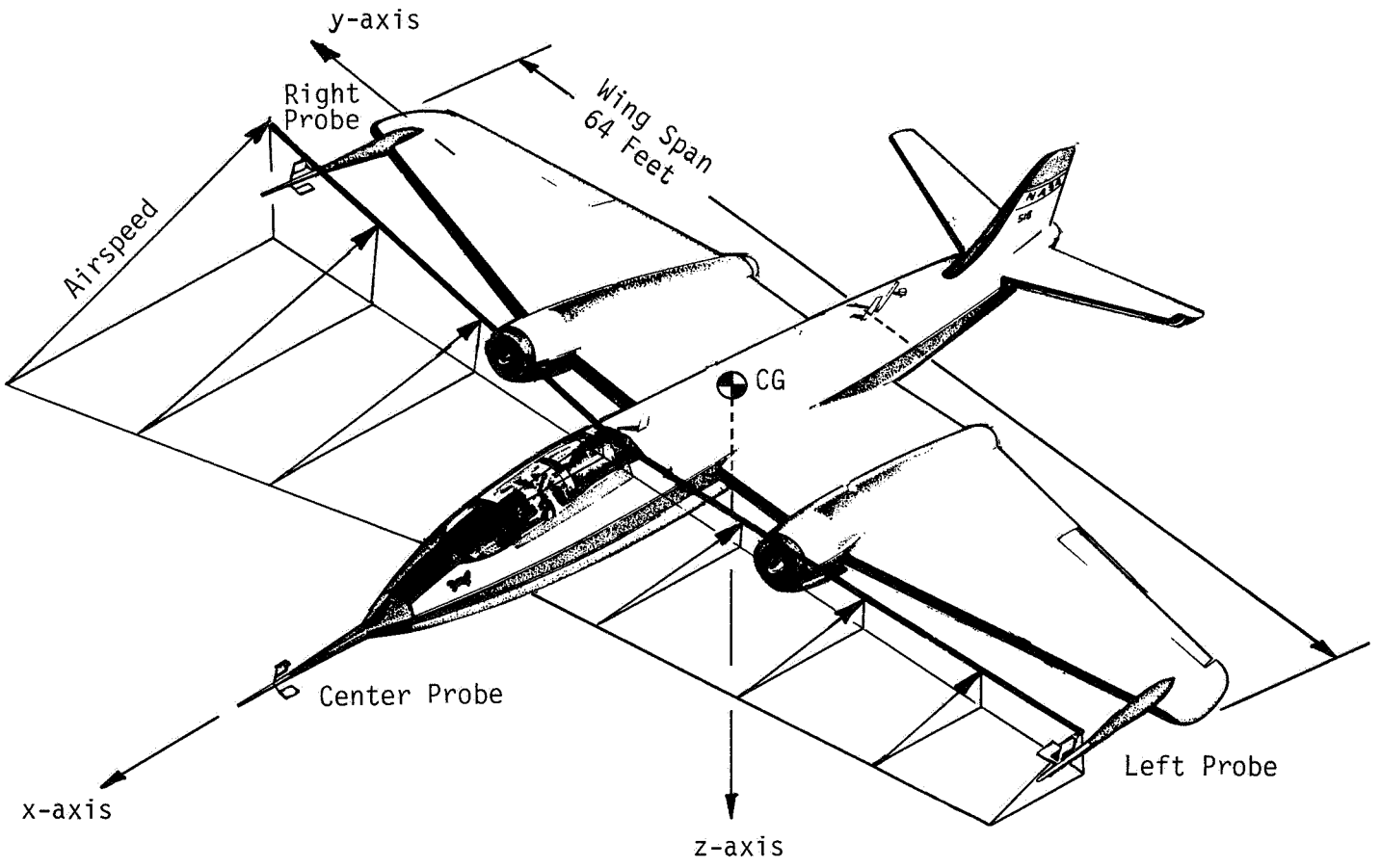

Figure 1.1. Spanwise variation of relative wind and angle of attack.

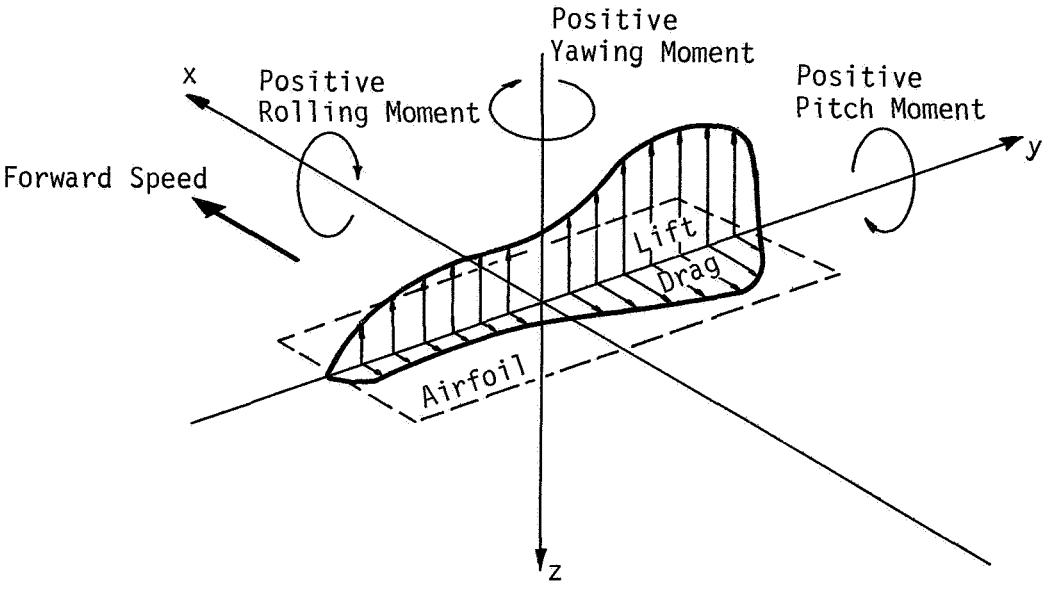

Figure 1.2. Asymmetric distributions of lift and drag.

Following, the procedure of introducing the strip theory calculations into the 6DOF simulation is explained in more detail. From 40 seconds of flight data lift, induced drag, and roll and yaw moment time histories are calculated based upon 0.25-second averages of the input parameters. The time histories of roll and yaw moments represent moments acting on the aircraft wing that would be unaccounted for if no spanwise variation in turbulence were considered. These moments are referred to as additional, and the roll moment expressed as:

$$L_{ADD} = \int_{-s}^{s} \ell(y) y dy \tag{1.1}$$

Similarly, the yaw moment is given by:

$$N_{ADD} = \int_{-s}^{s} d_i(y) y dy \tag{1.2}$$

where s is the half-span length and y is the lateral axis in the body axis coordinate system. The $\ell(y)$ and $d_i(y)$ indicate sectional lift and induced drag as a function of y.

Precalculated time histories of these two moments are then added into the force and moment equations in the 6DOF program (see Chapter IV). It is assumed that wing pitching moment is unaffected by the spanwise distribution of aerodynamic forces.* Furthermore, additional lift and induced drag are added as spanwise turbulence effects. The additional lift is given by:

$$L_{ADD} = L_{SPANWISE} - L_{UNIFORM} \tag{1.3}$$

and induced drag is expressed:

$$D_{i_{ADD}} = D_{i_{SPANWISE}} - D_{i_{UNIFORM}} \tag{1.4}$$

The subscript SPANWISE indicates total quantity of the aerodynamic force as calculated using strip theory with recorded variation in angle of attack and airspeed as input. The uniform terms come from a second calculation using strip theory, but this time the three separate measurements of the input parameters are averaged at each time step. These averages are then input to the strip theory model giving total lift and induced drag in a spanwise uniform wind field. Equations 1.3 and 1.4 thus are expressing the effect spanwise turbulence has on lift and induced drag.

---

*This is justified considering the negligible moment arm between aircraft center of gravity and the wing aerodynamic center. Changes in total lift due to spanwise turbulence are also small.

In Chapter II of this report the derivation of the strip theory is carried out. Chapter III contains the results of applying the strip theory to data from two test flights. The procedure for the 6DOF simulation of the test flights is described in Chapter IV. Results presented in Chapter IV demonstrate how spanwise turbulence effects influence the flight simulation of the B-57 aircraft. The last chapter contains the conclusions of this study.

CHAPTER II

DERIVATION OF STRIP THEORY

Vortex theory is the method most commonly used to calculate the lift and drag distributions of a finite wing. The strip theory developed in this chapter is a modified vortex theory which allows for random spanwise variations in angle of attack and airspeed. As the name implies, the airfoil is divided into a finite number of strips. At each strip, lift and drag can be evaluated. By integrating these forces across the wing span, the desired moments are obtained.

1. DERIVATION OF TOTAL QUANTITIES

The lift distribution across a wing can be represented by a distribution in the strength of the bound circulation $\Gamma(y)$ as shown in Figure 2.1. At any position in the spanwise direction, the lift per unit span can be expressed by Zhukovsky's theorem as (Kuethe and Chow 1976):

$$\ell(y) = \rho V(y)\Gamma(y) \tag{2.1}$$

where ρ is the air density and $V(y)$ is the speed of the wing along the direction of the x-axis in the wind coordinates. The frame of reference in wind coordinates is moving with the mean wind. The x-direction is chosen to be parallel to the direction of flight. Contrary to traditional analysis, $V(y)$ is considered a variable in the body axis y-direction. Similarly the induced (vortex) drag per unit span at any location again by Zhukovsky's theorem becomes:

$$d_i(y) = \rho w(y)\Gamma(y) \tag{2.2}$$

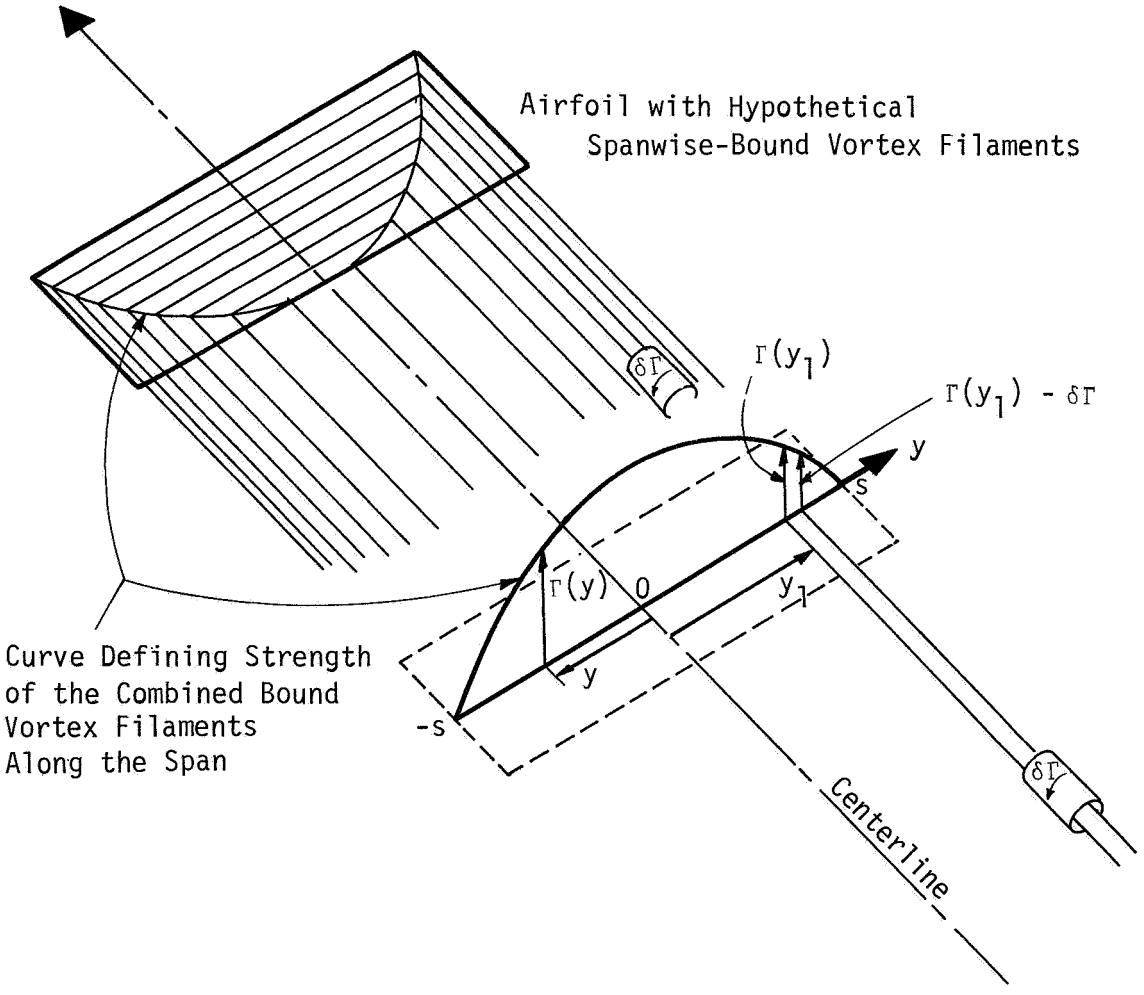

Figure 2.1. The relation between spanwise load variation and trailing vortex strength.

where w(y) is the downwash velocity. The total lift is found by integrating over the span:

$$L = \int_{-s}^{s} \rho V(y)\Gamma(y)dy \tag{2.3}$$

In the same manner, total induced drag is:

$$D_i = \int_{-s}^{s} \rho w(y)\Gamma(y)dy \tag{2.4}$$

As a first approximation, the circulation is often assumed to be elliptical in nature, which leads to closed form solutions of the integrals. In this study the integrals are solved numerically since the circulation can be non-elliptical and asymmetric.

The lift per unit span as in Equation 2.1 is also written:

$$\ell(y) = \frac{1}{2} \rho V^2(y)c(y)C_L(y) \tag{2.5}$$

where c(y) is the chord length and $C_L(y)$ is the sectional lift coefficient. Combining Equations 2.1 and 2.5 and solving for $\Gamma(y)$, the following expression is obtained:

$$\Gamma(y) = \frac{1}{2} V(y)c(y)C_L(y) \tag{2.6}$$

The continuation of the derivation is simplified by designating the variable y in terms of the angle θ as illustrated in Figure 2.2. Equation 2.6 is now written:

$$\Gamma(\theta) = 4sV(\theta)P_{shape}(\theta) \tag{2.7}$$

where P_{shape} is a dimensionless shape parameter which includes the variation in both lift coefficient $C_L(y)$ and the chord length c(y). The circulation is made proportional to four times the half-span length rather than the root chord length for convenience.

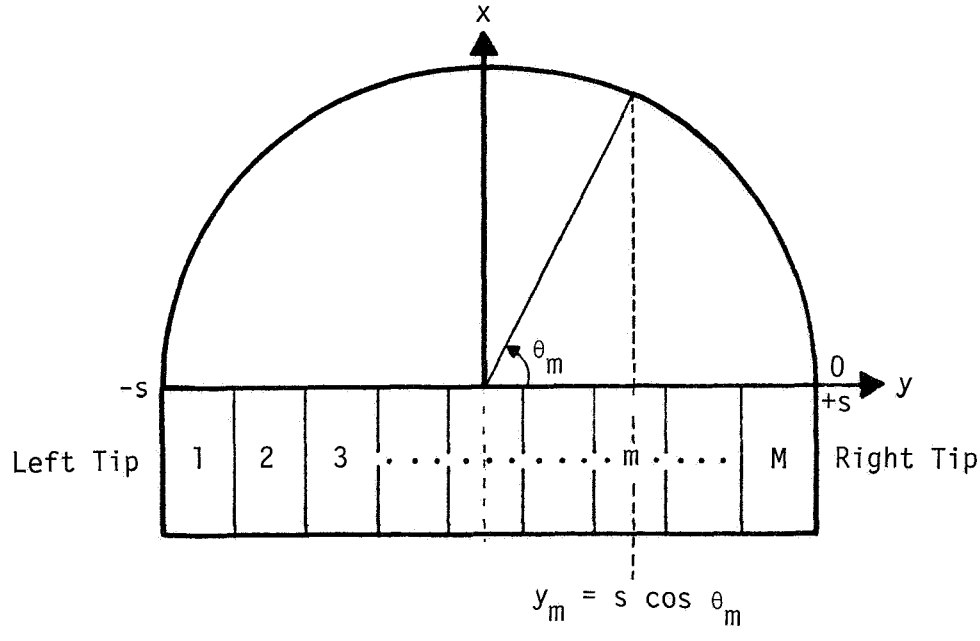

Figure 2.2. Change of variable.

The shape parameter is represented as a Fourier sine series:

$$P_{shape}(\theta) = \sum_{n=1}^{\infty} A_n \sin n\theta \tag{2.8}$$

The sine series satisfies the end conditions of the curve reducing to zero at the tips where $n\theta$ is zero or π (n is an integer). A_n is the amplitude of each sine curve making up the shape parameter. In Figure 2.3 a sample asymmetrical shape parameter is illustrated.

The total quantities of lift, induced drag, and roll and yaw moments given by Equations 2.3, 2.4, 1.1, and 1.2, respectively, are now written by substitution of Equations 2.7 and 2.8 as:

$$L = \sum_{n=1}^{\infty} A_n \int_0^{\infty} 4s^2 \rho V^2(\theta)(\sin n\theta \sin \theta)d\theta \tag{2.9}$$

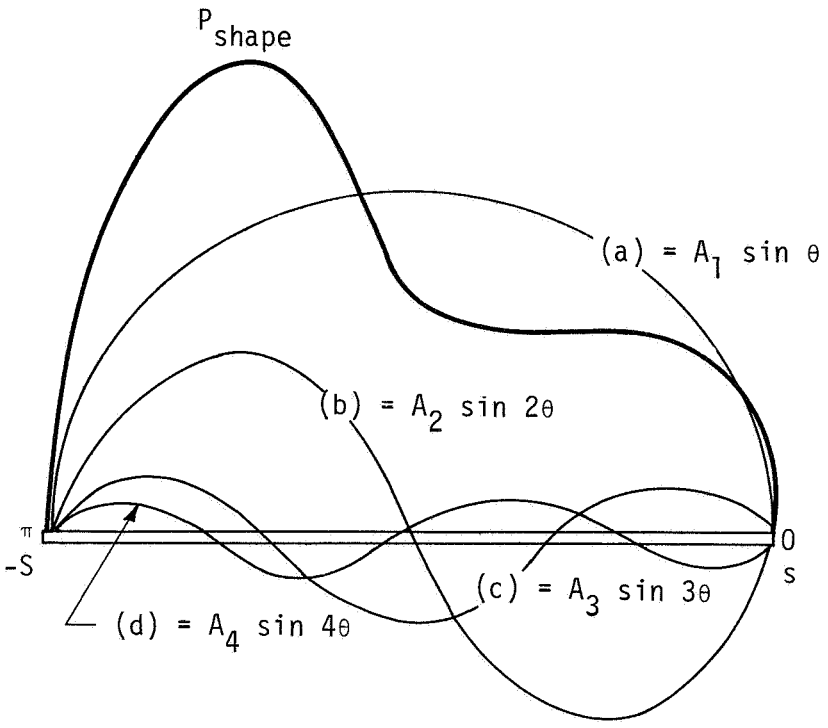

Figure 2.3. Loading as described by a shape parameter.

$$D_i = \sum_{n=1}^{\infty} A_n \int_0^{\infty} 4s^2\rho V(\theta)(\sin n\theta \sin \theta)w(\theta)d\theta \tag{2.10}$$

$$L_{ADD} = \sum_{n=1}^{\infty} A_n \int_0^{\pi} 4s^3\rho V^2(\theta)(\sin n\theta \sin \theta \cos \theta)d\theta \tag{2.11}$$

$$N_{ADD} = \sum_{n=1}^{\infty} A_n \int_0^{\pi} 4s^3\rho V(\theta)(\sin n\theta \sin \theta \cos \theta)w(\theta)d\theta \tag{2.12}$$

The change in variable going from y to θ is presented below:

$$\int_{-s}^{s} dy = \int_{\pi}^{0} \left(\frac{dy}{d\theta}\right)d\theta = \int_{\pi}^{0} (-s)\sin \theta \, d\theta = \int_{0}^{\pi} s \sin \theta \, d\theta \tag{2.13}$$

The obvious tasks then becomes to find solutions for the A_n coefficients as well as to evaluate the integrals in Equations 2.9 through 2.12. As already mentioned, the approach taken is to divide the wing into a finite number M sections (Figure 2.4). The integrals are then evaluated numerically using Simpson's rule. As will be explained in the following section, the number of A_n coefficients that can be solved for is the same as the number of strips, M. Thus, the Fourier series representation of P_{shape} is approximated to the desired accuracy by choosing a sufficiently large number M.

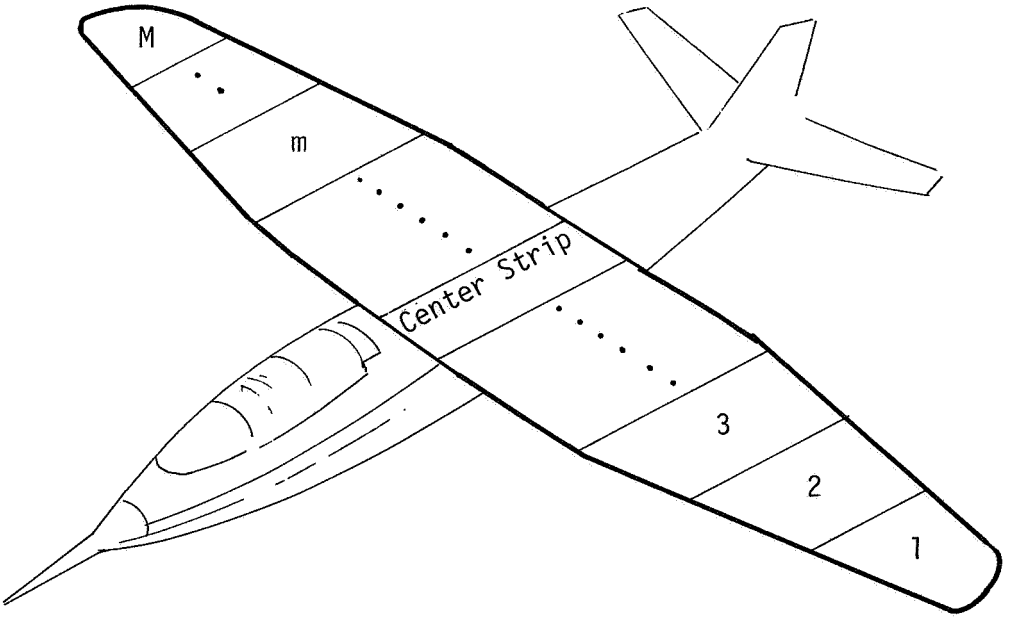

Figure 2.4. Division of wing into strips.

2. DETERMINATION OF THE A_n COEFFICIENTS AND DOWNWASH

The lift coefficient at a section y along the span in terms of the lift curve slope is given as:

$$C_L(y) = a_\infty[(\alpha(y) - \alpha_o(y)) - \varepsilon(y)] \tag{2.14}$$

where a_∞ is the two-dimensional lift curve slope; $\alpha(y)$ is the angle of attack; $\alpha_o(y)$ is the section zero lift angle; and $\varepsilon(y)$ is the downwash angle. Since wings commonly are designed with washout or a variable incidence angle, $\alpha_o(y)$ is written as a variable of y. The angle $\alpha_o(y)$ is negative and adds to the measured angle of attack $\alpha(y)$. The downwash angle $\varepsilon(y)$ is positive and reduces the effective angle of attack $\alpha_{eff}(y)$. The geometry of Equation 2.14 can be visualized by use of Figure 2.5.

Solving Equation 2.6 in terms of $C_L(y)$ and equating it with Equation 2.14 leads to the following result:

$$V(y)[\alpha(y) - \alpha_o(y)] = \frac{2\Gamma(y)}{c(y)a_\infty} + w(y) \tag{2.15}$$

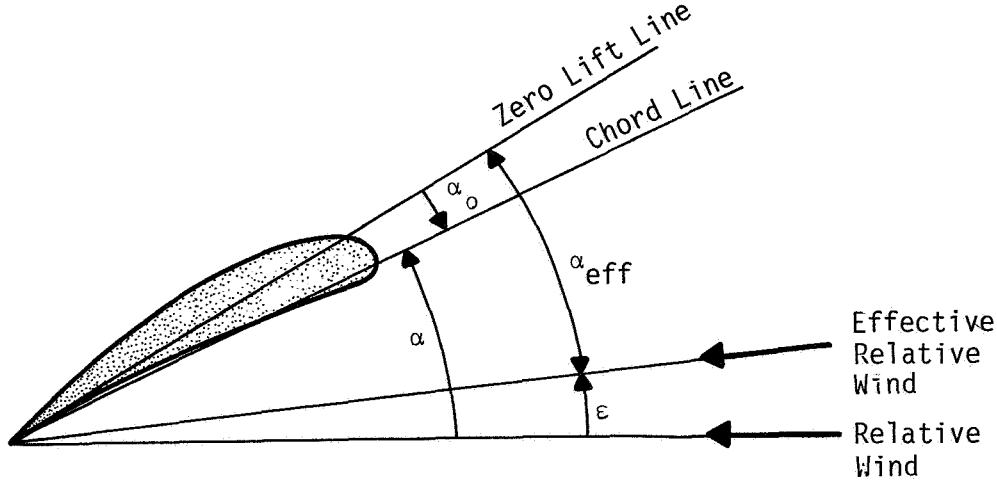

Figure 2.5. Effective angle of attack.

The downwash angle $\varepsilon(y)$ is given by:

$$\varepsilon(y) = \tan^{-1}\left[\frac{w(y)}{V(y)}\right] \tag{2.16}$$

Using a small angle approximation downwash becomes:

$$w(y) = V(y)\varepsilon(y) \tag{2.17}$$

The downwash term in Equation 2.15 must be expressed as a function of circulation before solutions to the A_n coefficients can be found. Using the Biot-Savart law, velocity induced at a point y due to a semi-infinite vortex line is given by:

$$v_i = \frac{\Gamma}{4\pi h} \tag{2.18}$$

where Γ is the circulation strength and h is the perpendicular distance from the vortex line to the point y (Figure 2.6). Consider now the influence on downwash at a position y along the span of the wing (Figure 2.1, page 7) due to a trailing vortex filament of strength $\delta\Gamma$ shed at y_1. Using Equation 2.18 this is expressed:

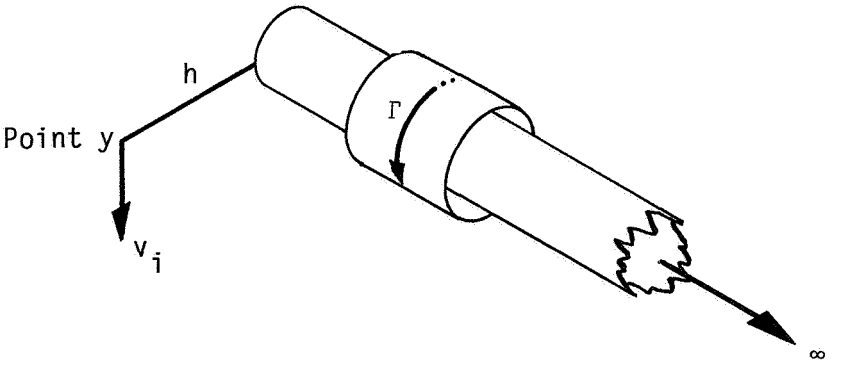

Figure 2.6. The Biot-Savart law.

$$\delta w(y) = \frac{-\dfrac{d\Gamma(y_1)}{dy_1}\, dy_1}{4\pi(y_1 - y)} \tag{2.19}$$

Since all trailing vortices influence the downwash velocity at position y, the total downwash is found by integrating Equation 2.19 across the span:

$$w(y) = -\frac{1}{4\pi} \int_{-s}^{s} \frac{\dfrac{d\Gamma(y_1)}{dy_1}\, dy_1}{y_1 - y} \tag{2.20}$$

Changing the variable and integrating Equation 2.20 by parts the downwash becomes.

$$w(\theta) = -\frac{1}{\pi} \int_{0}^{\pi} \frac{V(\theta_1) \sum_{n=1}^{\infty} A_n \sin n\theta_1 \sin \theta_1 \, d\theta_1}{(\cos \theta_1 - \cos \theta)^2} \tag{2.21}$$

Finally, by substituting Equation 2.21 into Equation 2.15 and expressing the circulation in terms of the Fourier series, the following equation is obtained:

$$\mu(\theta)[\alpha(\theta) - \alpha_o(\theta)] =$$

$$\sum_{n=1}^{\infty} A_n \left[\sin n\theta - \frac{\mu(\theta)}{\pi V(\theta)} \int_{0}^{\pi} \frac{V(\theta_1) \sin n\theta_1 \sin \theta_1}{(\cos \theta_1 - \cos \theta)^2} \, d\theta_1 \right] \tag{2.22}$$

where $\mu(\theta)$ is:

$$\mu(\theta) = \frac{c(\theta) a_\infty}{8s} \tag{2.23}$$

At this point in the derivation the finite number (M) strips are introduced. Assuming that $V(\theta)$, $c(\theta)$, $\alpha(\theta)$, and $\alpha_o(\theta)$ all are known at each

spanwise position m. Equation 2.22 is rewritten as:

$$\mu(\theta_m)[\alpha(\theta_m) - \alpha_o(\theta_m)] = \sum_{n=1}^{N} A_n \left[\sin n\theta_m - \frac{\mu(\theta_m)}{\pi V(\theta_m)} \int_0^{\pi} \frac{V(\theta_1) \sin \theta_1 \sin n\theta_1}{(\cos \theta_1 - \cos \theta_m)^2} d\theta_1 \right] \tag{2.24}$$

Solution to the A_n coefficients is then given by:

$$A_n = \sum_{M=1}^{M} \mu(\theta_m)[\alpha(\theta_m) - \alpha_o(\theta_m)] I_{nm}^{-1} \tag{2.25}$$

where I_{nm} is the matrix identifiable in Equation 2.24. Immediately, solutions of Equation 2.25 only exist when N equals M. Furthermore, the singularity inside the integral at $\theta_1 = \theta_m$ must be avoided. For most convenient numeric evaluation, I_{nm} is written:

$$I_{nm} = \sin n\theta_m - \mu(\theta_m) \left[\frac{n \sin n\theta_m}{\sin \theta_m} - \frac{1}{\pi V(\theta_m)} \int_0^{\pi} \frac{(V(\theta_1) - V(\theta_m)) \sin \theta_1 \sin n\theta_1}{(\cos \theta_1 - \cos \theta_m)^2} d\theta_1 \right] \tag{2.26}$$

The downwash given by Equation 2.21 can now be calculated at each of the spanwise sections as follows:

$$w(\theta_m) = \sum_{n=1}^{N} A_n \frac{V(\theta_m)}{\mu(\theta_m)} [I_{nm} - \sin n\theta_m] \tag{2.27}$$

3. COMPUTATION OF TOTAL QUANTITIES

Equations 2.11 and 2.12 can now be solved for L_{ADD}, and N_{ADD}, respectively. The quantities inside the integrals are all known at M

finite positions along the span. The integrals are then estimated numerically and the summations are performed with a finite number N A_n coefficients. Equations 2.9 and 2.10 are solved in a similar manner. The two solution sets, the first obtained using a spanwise distribution of airspeed and angle of attack and the second obtained using a uniform distribution, are then input into Equations 1.3 and 1.4, and the additional lift and drag forces are calculated.

In this study the wind is divided into 21 strips. Thus, the computations involved, in addition to estimating integrals numerically, include a 21 by 21 matrix inversion. A computer code written in Fortran has been developed to execute the large number of calculations.

CHAPTER III

STRIP THEORY CALCULATIONS

The reason for developing a strip theory with angles of attack and airspeed as spanwise variables is to utilize the data that has become available from the NASA Gust Gradient Program. Using the theory developed in the previous chapter, calculations of spanwise turbulence effects can now be performed. In this chapter the computation procedures are described and results presented.

1. DATA AVAILABLE

The NASA B-57 research aircraft is equipped to measure a large number of quantities. Table 3.1 lists all the variables directly recorded or calculated in the format received. Of interest in this part of the study are the angles of attack and airspeeds. The B-57 is capable of recording these values at three different positions. This is made possible by installing flow vanes and pitot tubes at each wing tip in addition to the nose (see Figure 1.1, page 2).

The variables are recorded on analog tapes at a rate of 200 per second aboard the airplane. Then at NASA Langley Research Center, Hampton, Virginia, digitized magnetic data tapes in engineering units are produced containing 40 sample points per second. In this study a 10-point averaging scheme is used resulting in four samples per second.

Each test flight consists of a number of runs. An individual run represents a continuous period of the flight at which data was recorded.

TABLE 3.1. Statistical Summary of Parameters Recorded on Flight 60, Run 18.

THE MAX,MIN,MEAN, AND RMS VALUES FOR EACH CHANNEL OF SERIAL NUMBER 3 FOLLOWS:

CHANNEL	UNITS	HIGH	LOW	MEAN	RMS	STD	POINTS
TIME	SECONDS	61185.608	61035.533	61110.57060	61110.58596	43.33377	6004.
PHI DOT	RAD/SEC	.175	-.290	-.00183	.05280	.05277	6004.
ACCL N CG	G UNITS	2.482	-.194	1.00663	1.03454	.23870	6004.
THETA DOT	RAD/SEC	.073	-.079	-.00269	.01140	.01107	6004.
THETA	RAD	.093	-.015	.04460	.04944	.02135	6004.
PHI	RAD	.179	-.258	.01150	.06534	.06432	6004.
PSI 1	RAD	359.118	-.155	347.43847	350.83069	48.67315	6004.
DEL PSI 1	RAD	2.701	-12.613	-4.31112	5.10750	2.73899	6004.
PSI 2	RAD	359.374	344.560	352.65590	352.66595	2.66272	6004.
DEL PSI 2	RAD	.962	-15.092	-4.07908	5.07909	3.02652	6004.
ACCL N LT	G UNITS	3.094	-1.062	1.09925	1.17582	.41740	6004.
ACCL N RT	G UNITS	3.347	-1.545	1.01530	1.10742	.44223	6004.
ACCL X CG	G UNITS	.187	-.044	.03026	.03708	.02142	6004.
ACCL Y CG	G UNITS	.121	-.155	-.01133	.03533	.03347	6004.
ALPHA CTR	RAD	.058	-.169	-.04786	.05286	.02244	6004.
BETA CTR	RAD	.050	-.174	-.05051	.05867	.02986	6004.
TEMP I	DEG F	59.947	59.048	59.57441	59.57472	.19304	6004.
TEMP P	DEG F	63.579	63.219	63.35632	63.35639	.09361	6004.
ACCL Z INS	G UNITS	2.448	-.177	1.01149	1.04024	.24286	6004.
ALPHA RT	RAD	.080	-.155	-.03612	.04343	.02411	6004.
BETA RT	RAD	.076	-.125	-.02053	.03323	.02613	6004.
ALPHA LT	RAD	.116	-.127	-.01360	.02792	.02439	6004.
BETA LT	RAD	.059	-.150	-.04308	.05082	.02695	6004.
PSI DOT	RAD/SEC	.101	-.078	-.00129	.02679	.02676	6004.
TEMP TOT	DEG C	20.476	15.957	18.10955	18.14388	1.11579	6004.
QC LT	PSID	1.220	.723	.92961	.93551	.10493	6004.
QC CTR	PSID	1.185	.721	.90358	.90931	.10196	6004.
QC RT	PSID	1.316	.779	.96044	.96654	.10841	6004.
PS	PSIA	11.488	11.379	11.41524	11.41526	.02327	6004.
TEMP IRT	VOLTS	4.609	3.359	4.46645	4.46885	.14621	6004.
HYGROM	DEG C	-20.140	-20.707	-20.40253	20.40276	.09688	6004.
QC2 LT	PSID	.100	-.117	.00019	.02324	.02324	6004.
QC2 CTR	PSID	.098	-.117	.00004	.02123	.02123	6004.
QC2 RT	PSID	.136	-.100	.00009	.02323	.02323	6004.
DAR	DEG	2.963	-2.203	1.20337	1.35712	.62747	6004.
DAL	DEG	2.885	-2.133	.29814	.63107	.55625	6004.
DELEV	DEG	1.211	-1.629	.14973	.40968	.38136	6004.
DSTAB	DEG	-.184	-.271	-.22094	.22118	.01017	6004.
DRUD	DEG	6.528	-1.706	1.47132	1.86019	1.13831	6004.
DTHRR	PCT MAX	65.918	55.469	59.89818	59.94931	2.47558	6004.
DTHRL	PCT MAX	62.402	52.441	56.94753	56.99567	2.34215	6004.
DELP	POSITION	1.000	.996	.99643	.99643	.00100	6004.
DSB	POSITION	.002	.000	.00195	.00196	.00003	6004.
D TO G	METERS	8724990.221	8721912.960	**********	**********	916.37648	6004.
B TO D	DEGREES	80.086	80.056	80.07075	80.07075	.00821	6004.
LONG	DEGREES	-105.277	-105.280	-105.27896	105.27896	.00109	6004.
LAT	DEGREES	40.066	39.914	39.99197	39.99199	.04360	6004.
TRK ANG	DEGREES	359.999	.002	130.35229	215.43624	171.53995	6004.
HDG	RADIANS	6.283	.000	6.08410	6.13840	.81474	6004.
VE	M/SEC	11.334	-6.138	1.28519	3.51669	3.27371	6004.
VN	M/SEC	122.446	103.442	111.82108	111.94539	5.27446	6004.
ALTITUDE	KM	2.106	2.030	2.08036	2.08042	.01637	6004.
TEMPC	DEGREES C	12.849	10.350	11.84025	11.84967	.47245	6004.
EW WND SPD	KNOTS	41.319	-9.162	10.56366	14.59437	10.07083	6004.
NS WND SPD	KNOTS	14.651	-19.233	-.12215	4.24683	4.24542	6004.
WIND SPEED	KNOTS	41.340	.044	12.26670	15.19971	8.97623	6004.
WIND DIREC	DEGREES	359.993	.091	245.89200	257.19053	75.39918	6004.
AIRSPEED R	M/SEC	134.803	104.464	115.44075	115.61524	6.35020	6004.
AIRSPEED C	M/SEC	128.139	100.604	112.06540	112.23505	6.16936	6004.
AIRSPEED L	M/SEC	129.915	100.713	113.62457	113.79647	6.25288	6004.
DELTA ALT	METERS	21.705	-54.721	-3.93629	16.83466	16.36936	6004.
INRTL DISP	METERS	16.440	-57.215	-5.56090	17.85698	16.97045	6004.
UG RIGHT	M/SEC	7.001	-10.846	.00000	2.18479	2.18498	6004.
UG CENTER	M/SEC	7.112	-10.385	.00000	2.03625	2.03642	6004.
UG LEFT	M/SEC	7.623	-10.927	.00000	2.08562	2.08579	6004.
VG RIGHT	M/SEC	752.132	-25.212	.34578	98.37485	98.38244	6004.
VG CENTER	M/SEC	733.269	-22.977	.32006	95.41415	95.42156	6004.
VG LEFT	M/SEC	741.958	-24.110	.28268	96.44861	96.45623	6004.
WG RIGHT	M/SEC	12.362	-16.573	-.02489	3.18635	3.18652	6004.
WG CENTER	M/SEC	10.405	-13.607	-.02681	2.80001	2.80011	6004.
WG LEFT	M/SEC	10.856	-13.847	-.03034	3.01159	3.01169	6004.

The length of a run may vary between less than half a minute and several minutes.

This first part of the study analyzes two runs originating from two separate flights. They have both been chosen because of high levels of turbulence. The first is Run 21 of Flight 6 recorded July 14, 1982, at Denver, Colorado, as part of the Joint Airport Weather Studies (JAWS) Project. The other is Run 18 of Flight 60 recorded February 1, 1984, at Boulder, Colorado, during the Orographic Effects Campaign. Additional information on the flights is listed in Appendix D. In these two runs the aircraft flew level flights approximately 1000 feet above the ground. The data tapes from Flight 60 include records of pilot control inputs but Flight 6 does not. For the response analysis in Chapter IV, this is of significance.

2. CALCULATION DESCRIPTION

The strip theory developed in Chapter II has been programmed in a computer code referred to as Program I. Inputs to this program are data files from the B-57 test flights containing time histories of angles of attack and airspeed at the three different spanwise positions. At each time step of the input file the strip theory calculations are performed. No aircraft dynamics enter into Program I; each time step is simply treated uniquely, neglecting unsteady effects. The output file is a time history of lift, induced drag, and roll and yaw moments equal in length to the input file. The rate at which calculations can be done on the Pixel Supermicro Motorola 68,000computer is substantially slower than required to keep up with inputs in real time. Each time step of

0.25 seconds will consume approximately one minute of computer time. This is largely due to the inversion of the sizable 21 by 21 matrix. The results of Program I are stored, and as described in Chapter IV, a dynamic response analysis based on these results is carried out.

The calculations in this chapter are designed so that the results can be directly utilized in FWG's six-degrees-of-freedom performance analysis computer program. The input to the 6DOF program representing spanwise turbulence is the quantities defined by Equations 1.1 through 1.4. Two iterations using the strip theory are necessary. In the first, the recorded linearized distribution of angle of attack and airspeed at each time step are input, see Figure 3.1. The first iteration yield time histories of L_{ADD}, N_{ADD}, $L_{SPANWISE}$, and $D_{i_{SPANWISE}}$. Next, in a second iteration, the calculations are based on inputs uniform across the span representing the average of the three spanwise recordings (Figure 3.2) uniquely determined at each time step. The second calculation gives $L_{UNIFORM}$ and $D_{i_{UNIFORM}}$ but no moments as they vanish when the distribution in lift and drag are symmetric. The two iterations using the strip theory then give the time histories of the four quantities representing spanwise turbulence needed for the response analysis.

3. ANALYSIS OF STRIP THEORY RESULTS

In the analysis of strip theory results, two problems were uncovered. First, the value of lift calculations appeared to be exaggerated as a result of neglecting unsteady effects. Secondly, the angles of attack seemed to contain a constant offset. The methods used to solve these complications are presented preceding the final results in this section.

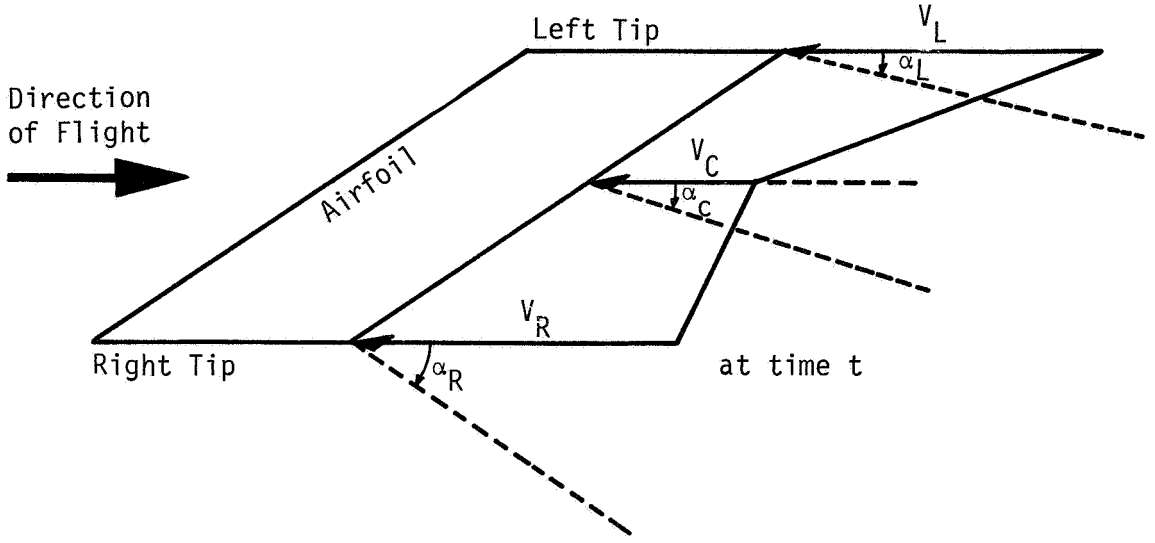

Figure 3.1. Sample of a linear distribution of inputs to Program I.

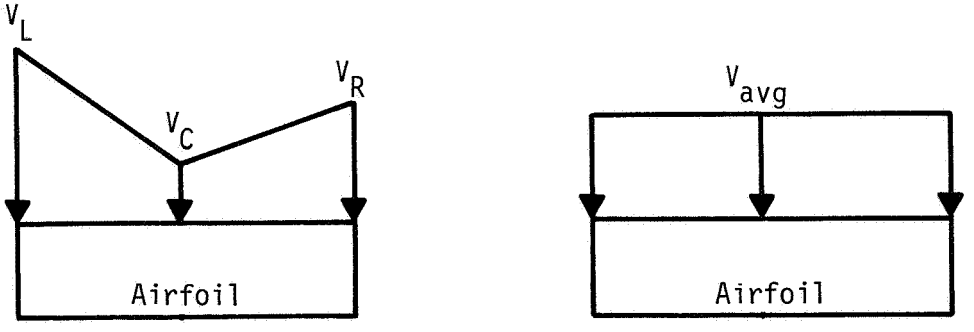

Spanwise airspeed distribution Uniform airspeed distribution

Figure 3.2. Spatial and uniform spanwise distributions of airspeed.

At each step of the calculations in Program I a steady-state condition is assumed. It would then be expected that the instantaneous lift and drag values are overestimated in gusts. A short literature review led to the estimation of a gust alleviation factor K, accounting for unsteady effects. This factor K = 0.7 is applied to the results as described in Appendix A.

A second complication attributed to the inclination angles of the probes on the B-57 introduces offsets in the recorded angles of attack. Because of unrealistic results from the calculations applied to Run 18 of Flight 60 an investigation was initiated. It showed that the time-averaged angle of attack for Flight 60, Run 18, differs between the three recording probes. Specifically, the left probe indicates an angle of attack about two degrees higher than the center probe, whereas the right probe lies close to half of a degree below on a time-averaged basis. Moments calculated with Program I are of varying magnitude but suspiciously of only on polarity. This is not in accordance with expectations, namely moments varying in both directions. This problem is avoided by correcting the angles of attack data by a constant value representing the difference of the time-averaged values. Several runs of Flight 60 represent the basis for estimating these correction values. The left probe angle of attack is reduced by 2.02 degrees and the center probe reduced by 0.67 degrees. Figure 3.3 shows the angles of attack as recorded during a 50-second period of Flight 60, Run 18, and Figure 3.4 shows angles of attack with the corrections included.

The first direct result of strip theory calculations is shown in Figure 3.5. Using the spanwise linear distribution, the lift divided by

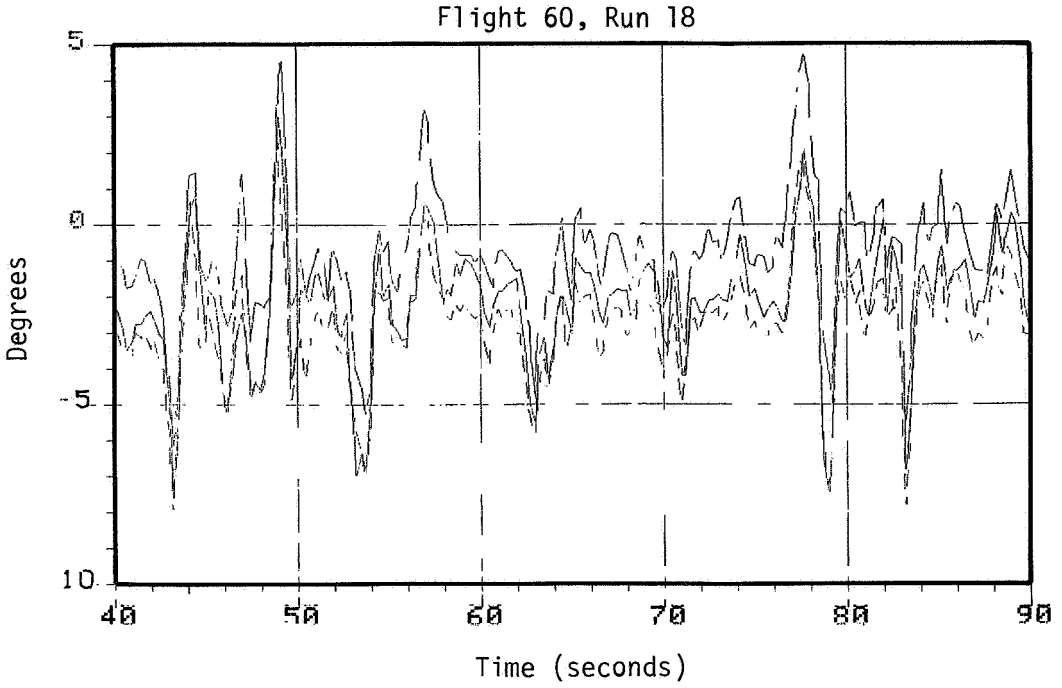

Figure 3.3. Recorded angles of attack.

—— Center Probe
----- Right Probe
— — Left Probe

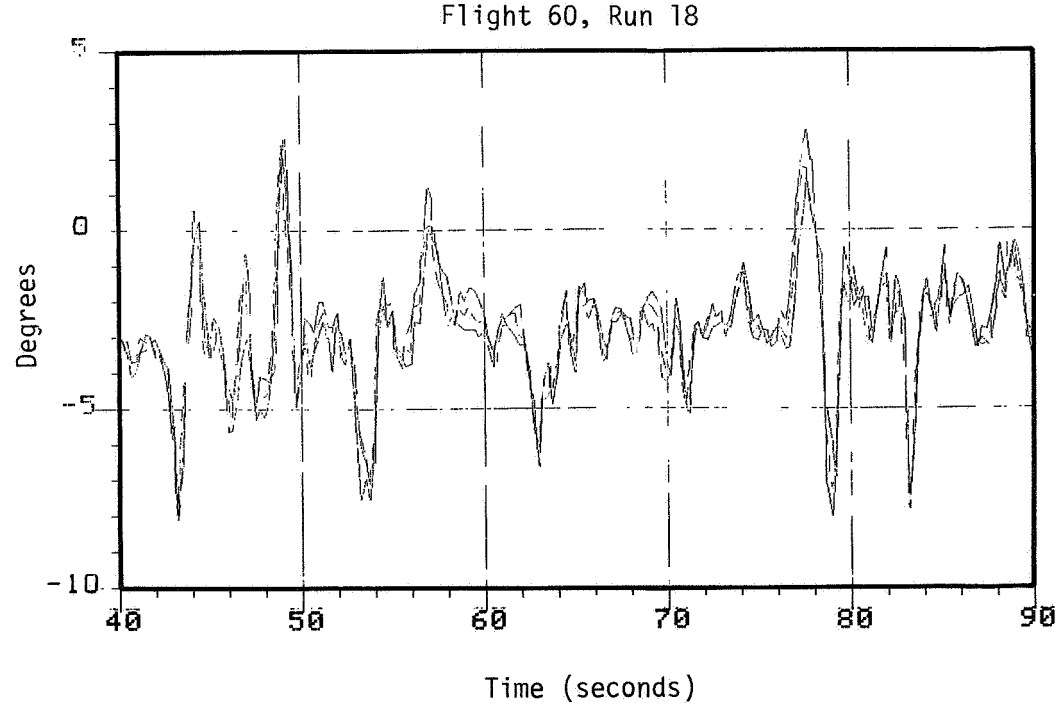

Figure 3.4. Corrected angles of attack.

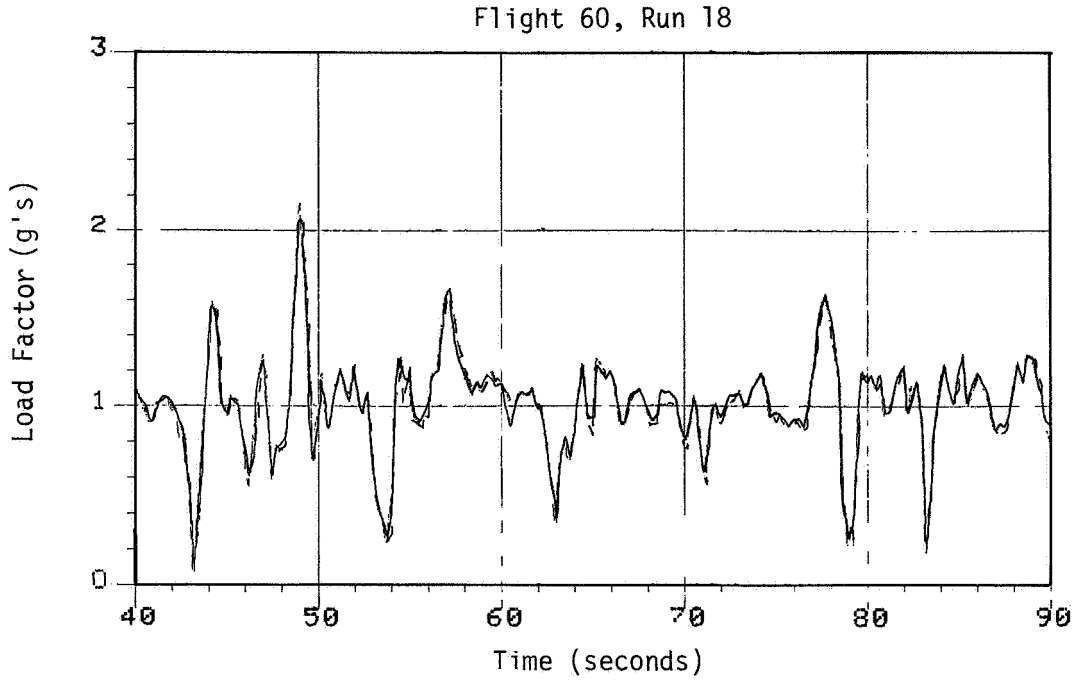

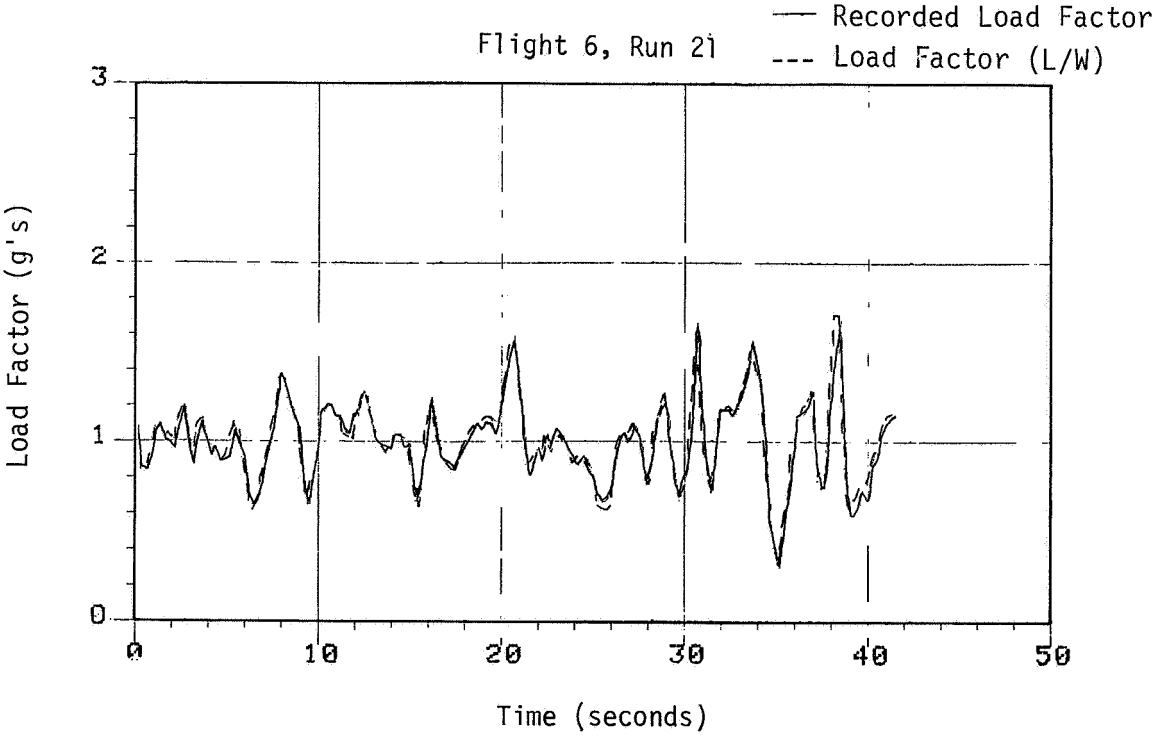

Figure 3.5. Strip theory load factor calculations.

weight obtained in the first calculations with Program I is plotted. The lift is normalized with aircraft weight. The aircraft lift-to-weight ratio is computed and is compared with a plot of load factor recorded by the on-board inertial navigation system (INS) in the figure. The theoretical lift-to-weight ratio is computed independently of the INS and is based on data collected by use of pitot tube and angle of attack probes. Any dynamic influence on lift is neglected; but, since the test flight is close to being level and unaccelerated, the dynamic terms are expected to be small. The agreement between the two curves suggest the strip theory model is reliable in estimating lift on a wing. Note that the entire 41.5-second Run 21 of Flight 6 is analyzed, whereas only a 50-second period inside the total 140-second Run 18 of Flight 60 is studied. The first 40 seconds of Run 18 of Flight 60 is omitted as is indicated by the time variable of that run in the figures. Also, the mean airspeed of Flight 60, Run 18, is 113 m/s but 96 m/s in Flight 6, Run 21. With the independent variable as distance (i.e., $x = Vt$), the abscissa would be approximately 15 percent elongated in a plot of Flight 60.

Figure 3.6 represents the L_{ADD} in Equation 1.3, which is computed as the difference of the two calculations illustrated schematically in Figure 3.2. The lift difference is generally small but can reach values up to 10 percent of the weight. The problem with offset due to the discrepancy in angle of attack between probes is corrected in Flight 60, Run 18, but not in Flight 6, Run 21. This can explain the apparent negative time-averaged L_{ADD} in Flight 6, Run 21. It is a result of an approximately one half of a degree lower time-averaged angle of attack

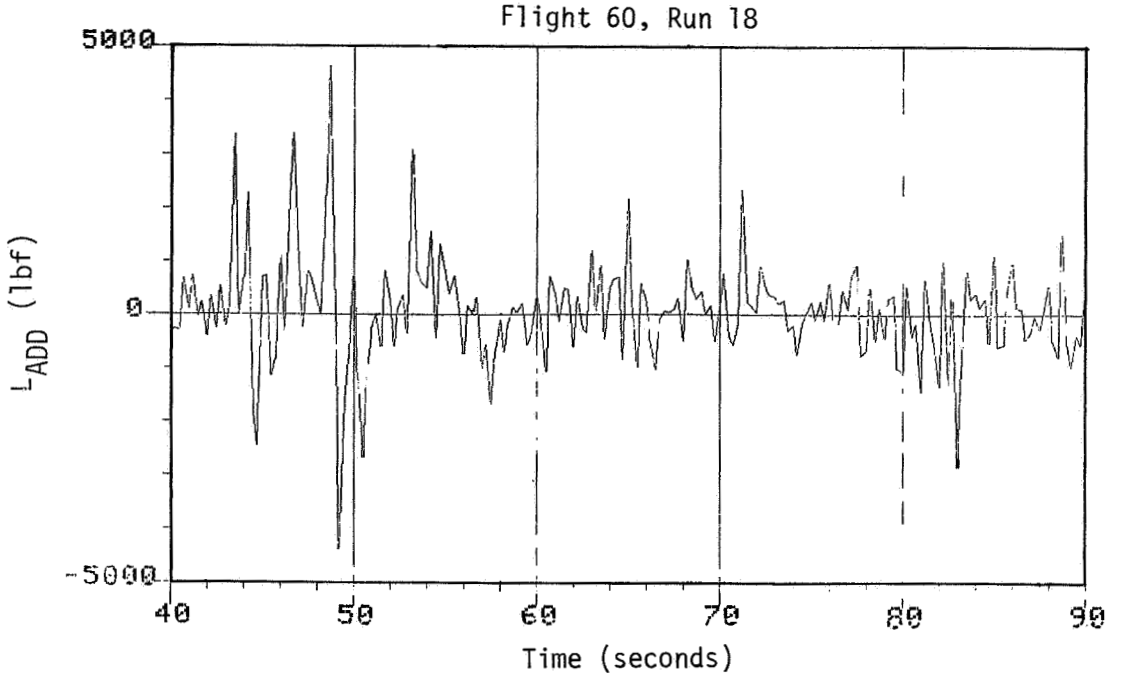

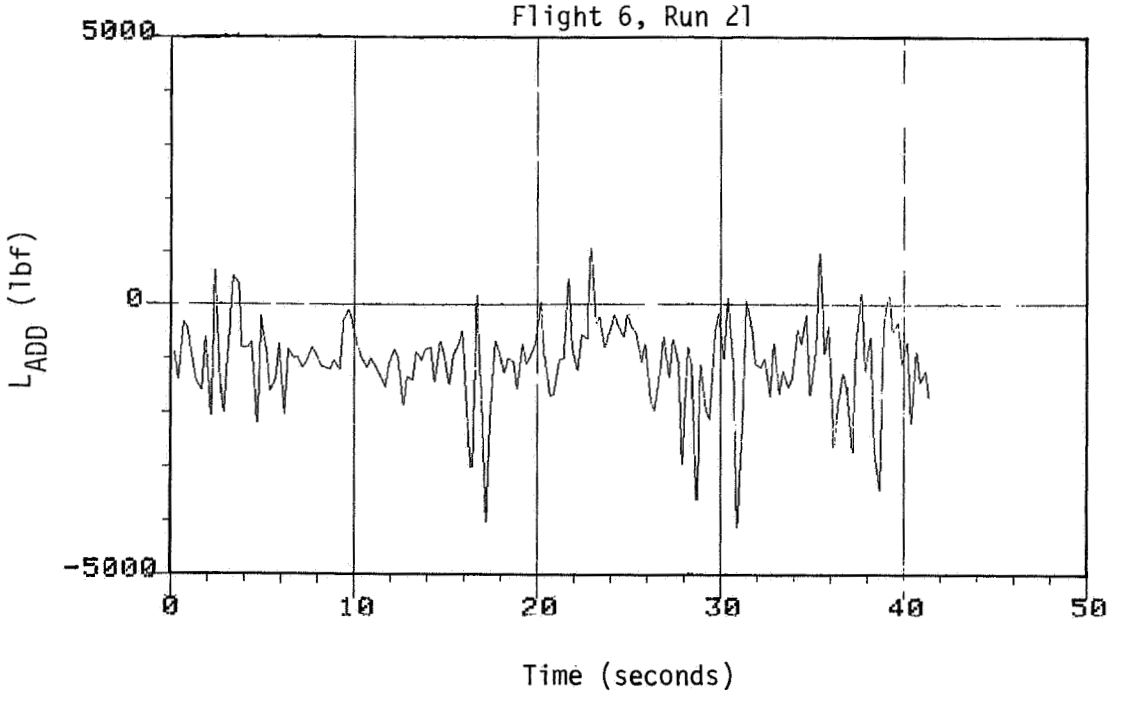

Figure 3.6. Additional lift due to spanwise turbulence.

recorded in the nose of the aircraft, see Figure 3.7. This makes the time-averaged lift with uniform distributions greater than the time-averaged lift with spanwise distributions which results in the negative difference. In this case this difference may simply be caused by upwash at the wing tips and not an inclination induced error in the center probe.

Figure 3.8 is identical to Figure 3.6 except that induced drag not lift is plotted. D_{ADD} is much smaller which is anticipated.

The roll moment L_{ADD} in Equation 1.1 due to spanwise turbulence is shown in Figure 3.9. The mean value of L_{ADD} in Flight 6, Run 21, is negative because of the only slightly higher time-averaged angle of attack on the right wing tip compared to the left wing tip. As noted, this asymmetry is also displayed in Figure 3.6, and could possibly be real because of the relatively short time period over which the calculation is made. The roll moment of Flight 60, Run 18, in Figure 3.9 is based on the corrected angles of attack as previously mentioned

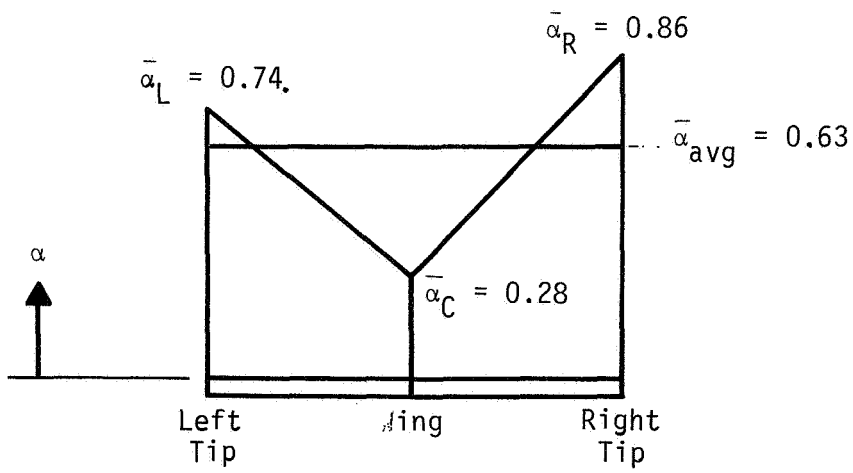

Figure 3.7. Time-averaged angles of attack for Flight 6, Run 21.

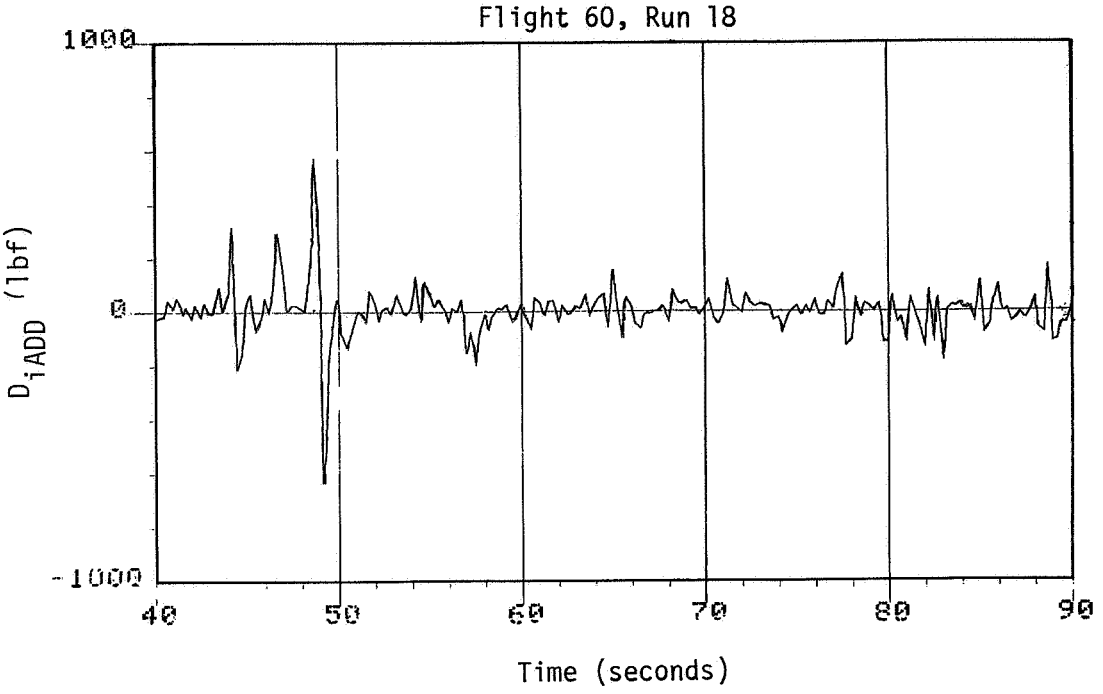

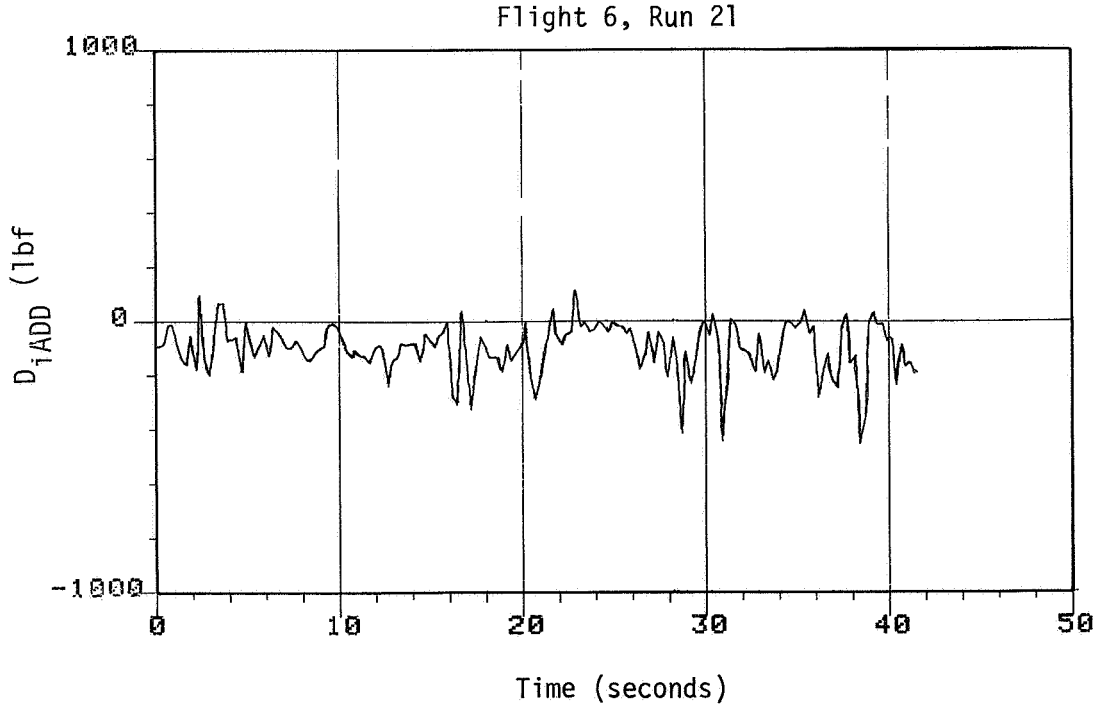

Figure 3.8. Additional induced drag due to spanwise turbulence.

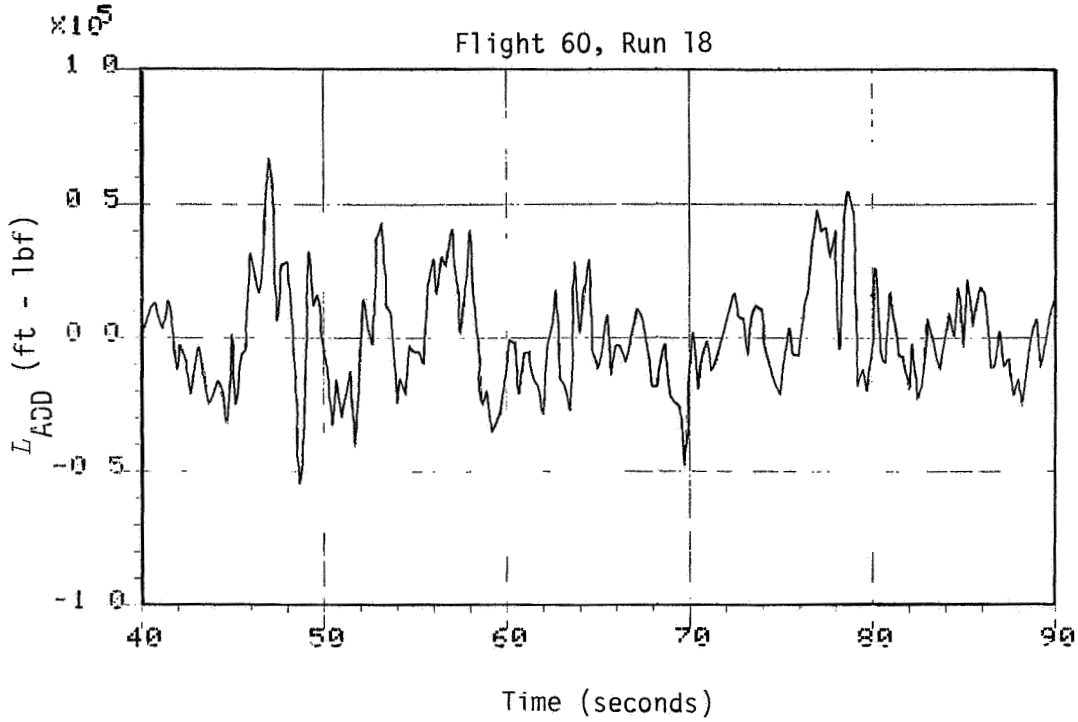

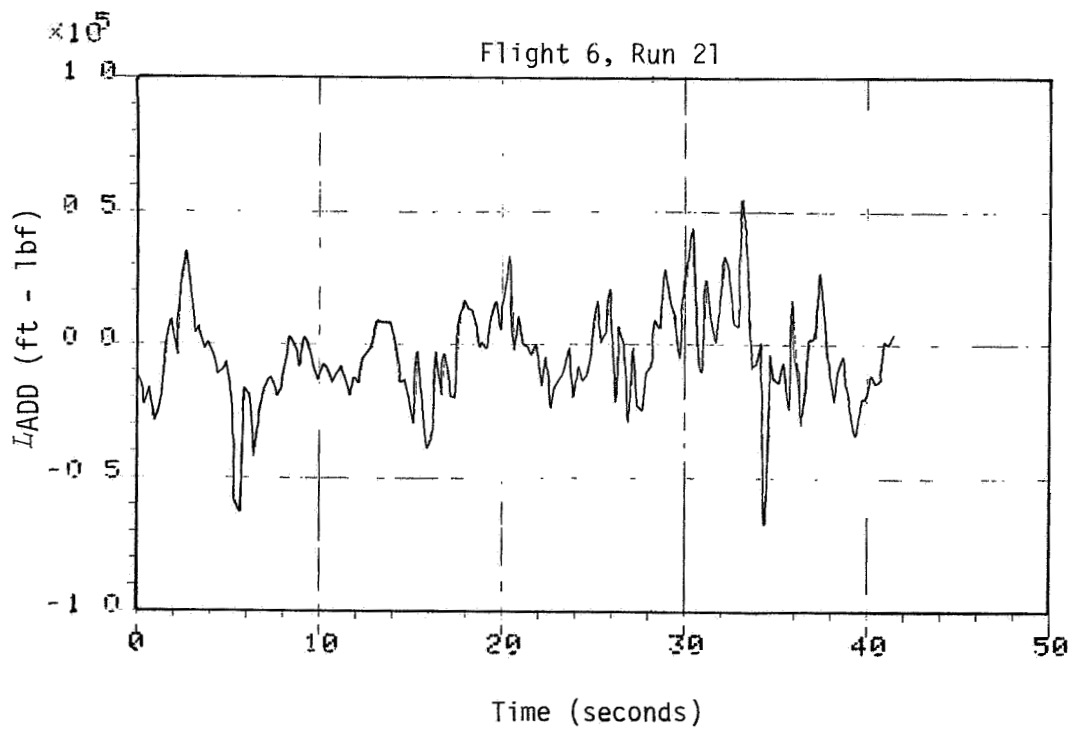

Figure 3.9. Computed additional roll moment due to spanwise turbulence.

(Figure 3.3, page 23). Similar results for the yaw moment due to spanwise turbulence is presented in Figure 3.10.

The magnitudes of L_{ADD} and N_{ADD} are of little meaning unless they are weighed against known quantities. To provide the reader with a feel for the magnitudes of these values, the roll moment developed as a function of aileron input and yaw moment due to a rudder deflection are plotted in Figure 3.11. It shows the equivalent to the largest roll moment in Figure 3.9 is equivalent to about 10 degrees aileron input. Similarly, the yaw moments due to spanwise turbulence can reach magnitudes comparable with a 3 degree rudder deflection, Figure 3.12. Figures 3.11 and 3.12 were generated using the aileron control power $C_{\ell_{\delta_a}}$ and the rudder control power $C_{n_{\delta_r}}$ coefficients listed in Appendix B.

The second part of this study investigates the influence on airplane performance generated by the four quantities L_{ADD}, D_{iADD}, L_{ADD}, and N_{ADD}.

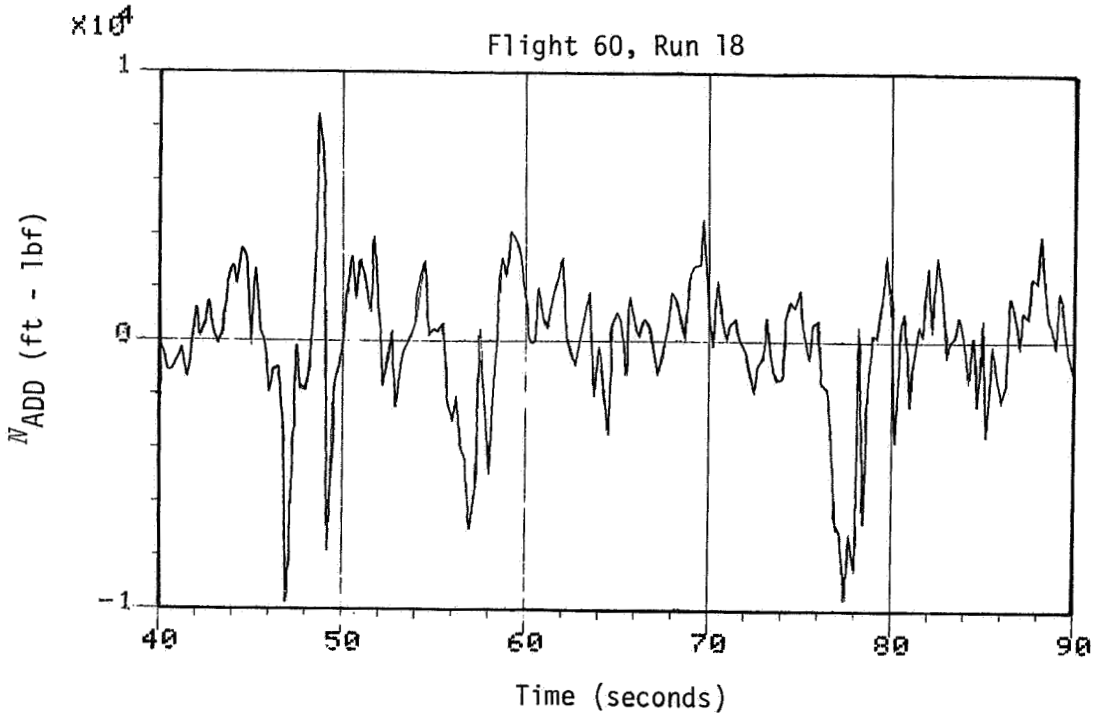

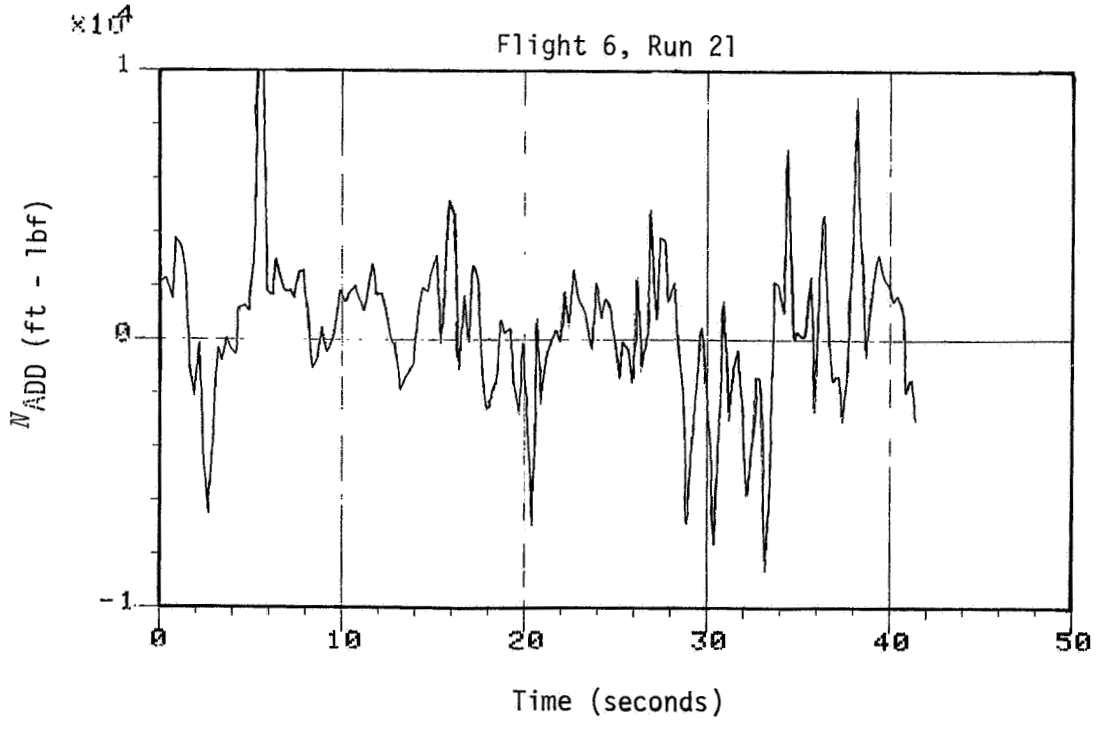

Figure 3.10. Computed additional yaw moment due to spanwise turbulence.

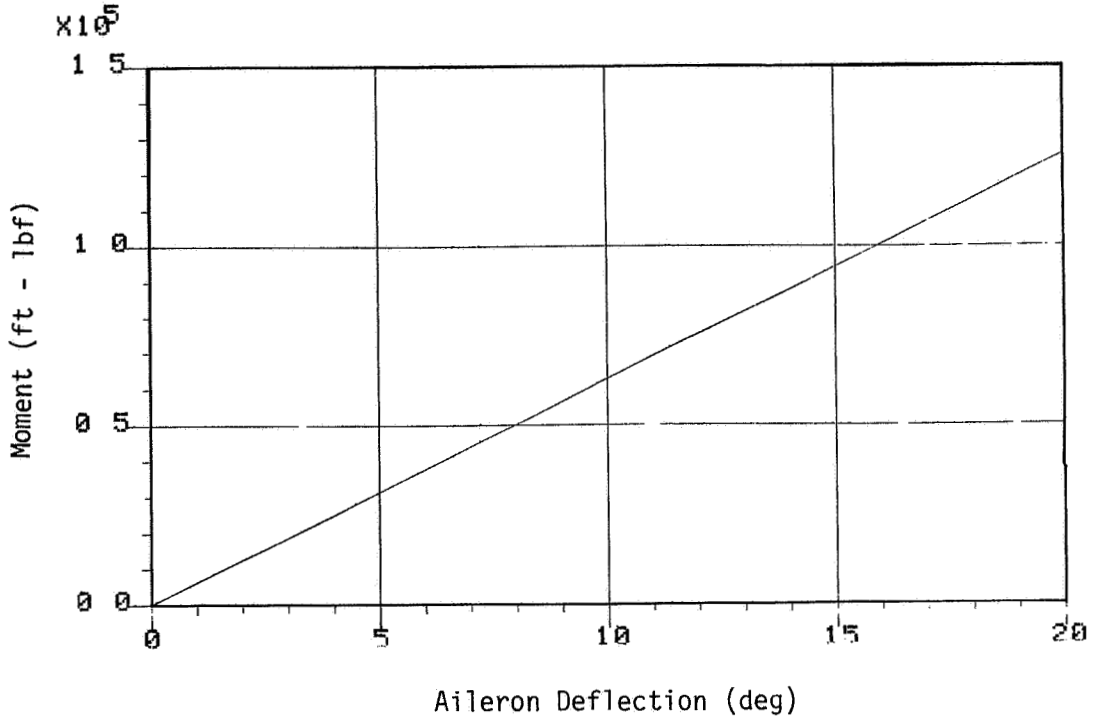

Figure 3 11. Roll moment by use of aileron.

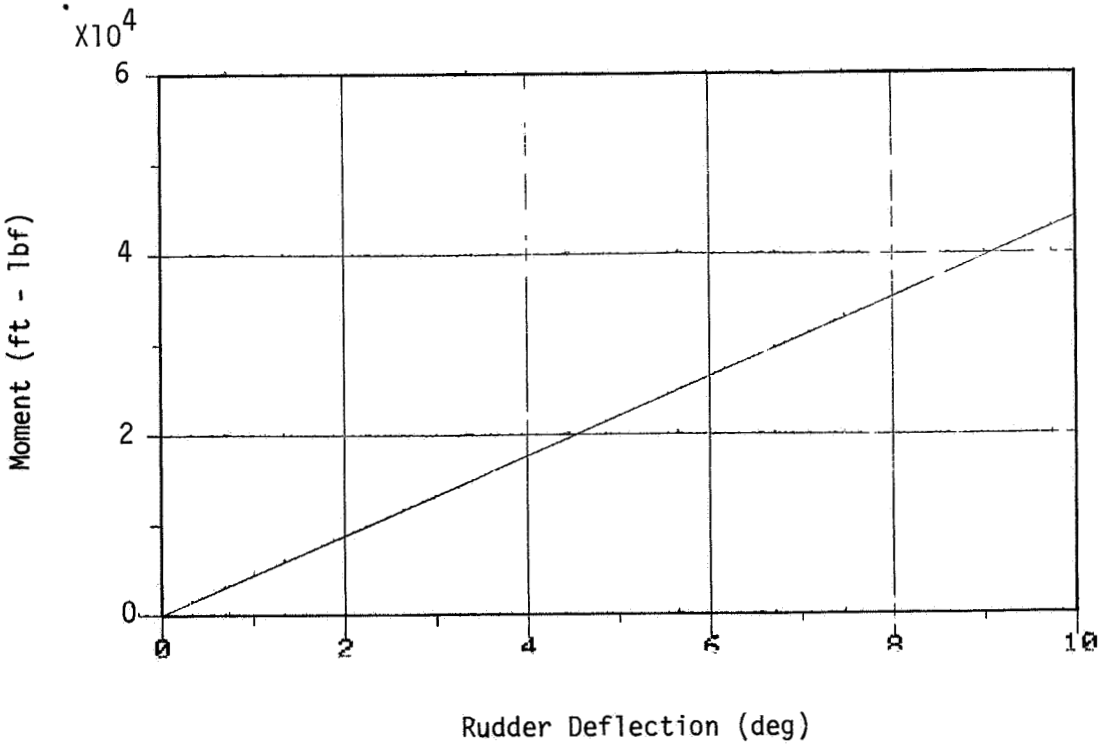

Figure 3.12. Yaw moment by use of rudder.

CHAPTER IV

FLIGHT SIMULATION USED TO EVALUATE RESPONSE EFFECTS

In the first part of the study, time histories of aerodynamic forces and moments on the wing due to spanwise turbulence are computed. In the second part, the effects of spanwise turbulence on the wing are incorporated into a 6DOF flight simulation to investigate aircraft response. The methods and results of the second part are given in this chapter.

1. IMPLEMENTING SPANWISE TURBULENCE

A second computer code is used to implement spanwise turbulence into aircraft response analyses. This program is FWG's six-degrees-of-freedom flight simulation routine. The wind variation measured during a given flight is used as an input to the computer program. The computed flight trajectory parameters are then compared to those measured by the INS system on the actual airplane when encountering the same wind.

Two sets of calculations are employed. First a reference case which does not include spanwise variations is computed. For the reference case only the wind variation measured by the central boom is input to the 6DOF program. This wind is assumed to vary with time but to act uniformly over the entire aircraft. Next the program is modified to include the results of spanwise variation based on the strip theory calculations described earlier. In this manner, a comparison of the two sets of results can be carried out to assess the influence of spanwise variation. Figure 4.1 is a block diagram outline of the procedure for the aircraft performance analysis.

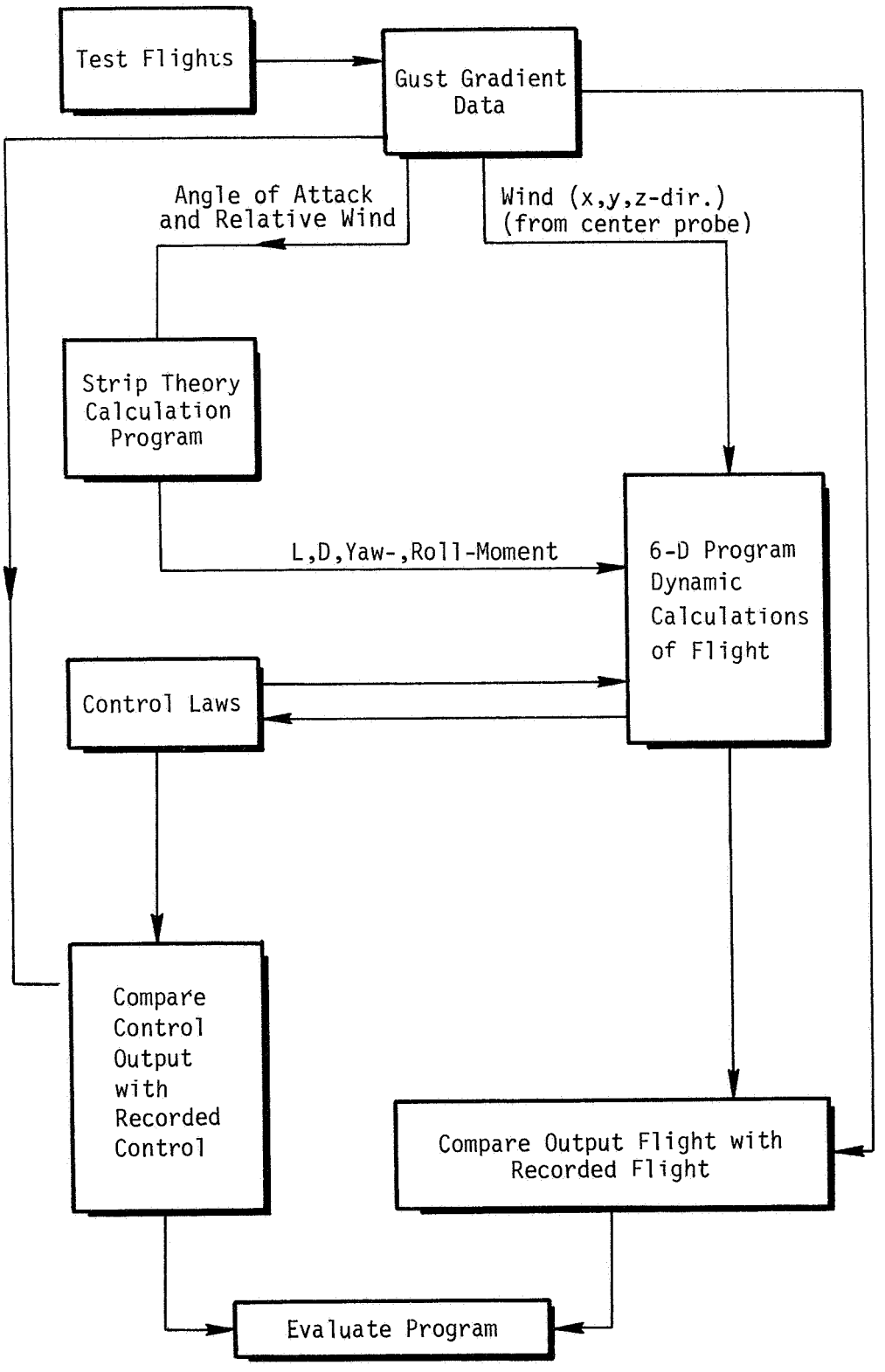

Figure 4.1. Outline of analysis procedure.

The 6DOF program is the same as used in a study by Frost et al. (1984). The original program includes wind gradients in the equations of motion (Frost and Bowles 1984), but for this purpose gradients are neglected. The only other modification is the incorporation of spanwise turbulence. This is achieved by simply adding the four terms (Equations 1.1 through 1.4) which account for spanwise turbulence into the force and moment equations of the 6DOF program, Equations 4.1 through 4.61

$$L = \frac{1}{2}\rho V^2 S(C_{L_o} + C_{L_\alpha}\alpha + C_{L_{\delta_e}}\delta_e + C_{L_q}q + C_{L_{\dot{\alpha}}}\dot{\alpha}) + L_{ADD} \tag{4.1}$$

$$D = \frac{1}{2}\rho V^2 S(C_{D_o} + C_{D_\alpha}\alpha + C_{D_{\delta_r}}\delta_r + C_{D_{\delta_a}}\delta_a) + D_{iADD} \tag{4.2}$$

$$F_Y = \frac{1}{2}\rho V^2 S(C_{Y_\beta}\beta + C_{Y_{\delta_r}}\delta_r) + L \sin\phi \tag{4.3}$$

$$L = \left(C_{\ell_\beta}\beta + C_{\ell_{\delta_r}}\delta_r + C_{\ell_{\delta_a}}\delta_a + C_{\ell_p}\frac{pb}{2V} + C_{\ell_r}\frac{rb}{2V}\right)\frac{1}{2}\rho V^2 Sb + L_{ADD} \tag{4.4}$$

$$M = \left(C_{m_o} + C_{m_\alpha}\alpha + C_{m_{\delta_e}}\delta_e + C_{m_q}q + C_{m_{\dot{\alpha}}}\dot{\alpha}\right)\frac{1}{2}\rho V^2 Sb \tag{4.5}$$

$$N = \left(C_{n_\beta}\beta + C_{n_{\delta_r}}\delta_r + C_{n_{\delta_a}}\delta_a + C_{n_p}\frac{pb}{2V} + C_{n_r}\frac{rb}{2V}\right)\rho V^2 Sb + N_{ADD} \tag{4.6}$$

Only pitching moment in Equation 4.5 remains unaffected by the spanwise turbulence, whereas side force in Equation 4.3 is coupled with Equation 4.1 and thus influenced by changes in lift due to spanwise turbulence. The incorporation of precalculated time histories of spanwise turbulence effects into the 6DOF flight simulation is acceptable subject to the following condition. The computer simulation must closely resemble the real test flight from which spanwise turbulence is calculated. In this case, the test flight is a straight level flight with only small

pertubations from the trim condition, and thus relatively easy to simulate. Two simulations of the test flight, one including spanwise turbulence and one without, are performed to reveal the effect of spanwise turbulence on aircraft response.

Note, the following assumption applies to the computer simulation. The 6DOF program regards the aircraft as a perfect rigid body. The corresponding error introduced is expectedly less for the B-57 than for a high aspect ratio wing airplane. The air density and the weight of the B-57 is assumed to be constant. Furthermore, the aerodynamics of the B-57 are represented by aerodynamic coefficients (Appendix B) that are assumed to be linear over the range they are used. The airplane is controlled through the use of the simple linear gain automatic control algorithms. The mathematical control laws are explained in further detail in Appendix C.

2 DATA UTILIZED

From the B-57 Gust Gradient Program flight data, many test flights are available. The immense number of flight parameters recorded during a test flight is shown in Table 3.1, page 18. Early flights, however, lacked recordings of pilot control inputs. In the second part of this study, such records can be useful for comparison of computed and measured results, and consequently Flight 60 was chosen as it became available in the spring of 1984. Flight 6 dates back to 1982 and does not contain pilot control records and is not analyzed any further.

In the strip theory calculations, the three angles of attack and the corresponding airspeeds are utilized. In the 6DOF simulation program the atmospheric conditions measured on Flight 60, Run 18, are used. Air

density is calculated from temperature and static pressure. The wind components are obtained by removing aircraft motion, measured with the INS system, from sensor measurements. the atmospheric inputs including wind and density are used to reconstruct conditions of the test flight.

3. RESULTS OF 6DOF FLIGHT SIMULATIONS

This section presents the results of the 6DOF flight computer simulations of Flight 60, Run 18. The two calculations, one incorporating spanwise turbulence and one without, are both plotted on the same graph to make comparison easy.

The three wind components of Flight 60, Run 18, as measured with the INS during the flight are plotted in Figures 4.2, 4.3, and 4.4. Figure 4.3 shows the airplane encountered a strong sidewind a few seconds into the time period considered of the test run.* The strong changes in north/south wind occurring around the 50-second mark (Figure 4.4) not surprisingly produce the strongest spanwise turbulence reflected in L_{ADD} in Figure 3.6, page 26.

In Figure 4.5 the recorded yaw angle on Flight 60, Run 18, is plotted. About 43 seconds into the run the yaw angle reaches roughly negative 11 degrees indicating the nose pointing to the left. This is predictable and expected as the airplane entered a strong sidewind from the left at that point in time, see Figure 4.3. The recorded airplane response is relevant in this context to serve as reference state that computer predicted response can be compared with. Refering to Figure 4.6, it is demonstrated that the computer simulation of Flight 60, Run 18, compares favorably with the actual flight. Figure 4.6 also

---

*Note that the airplane heading is due north on Flight 60, Run 18.

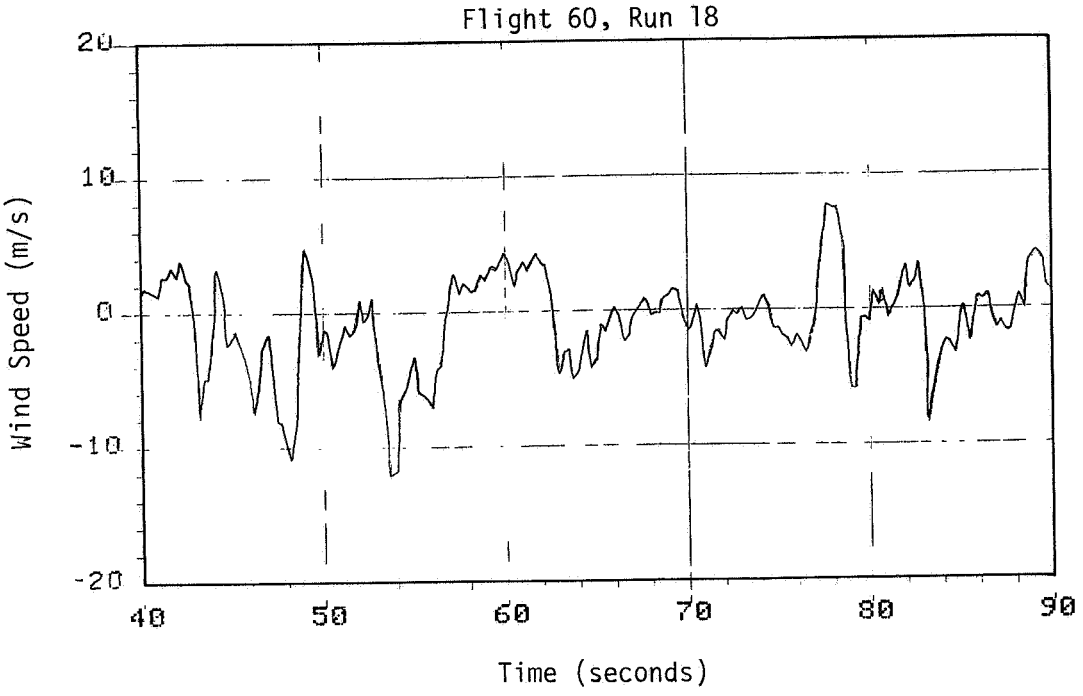

Figure 4 2 Vertical wind component

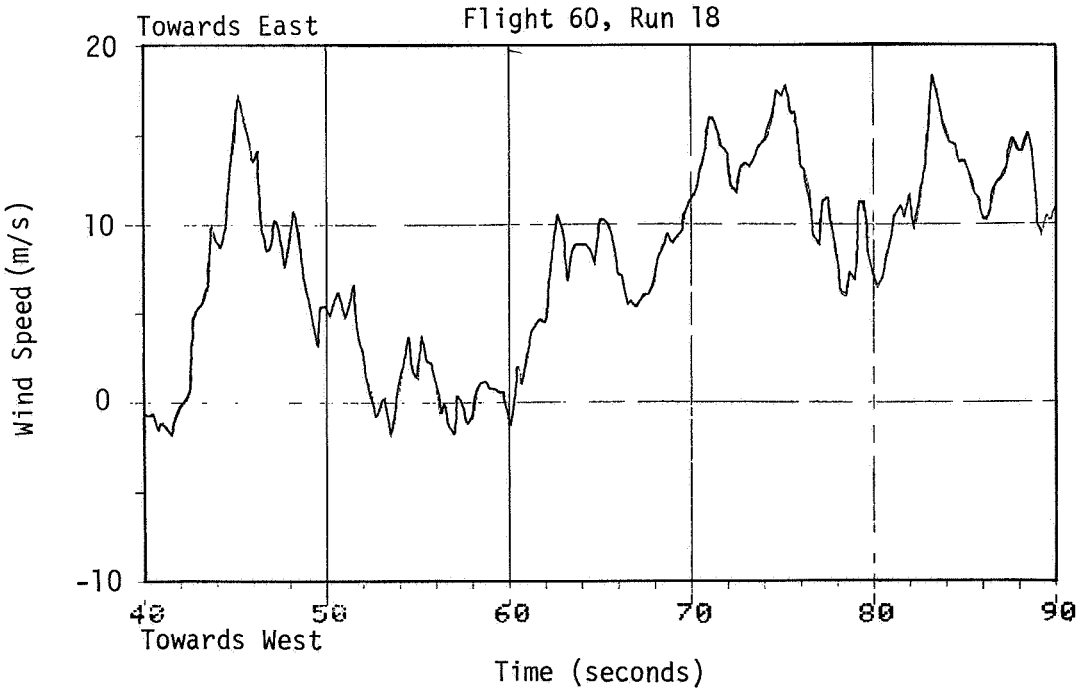

Figure 4.3. Lateral wind component (east/west).

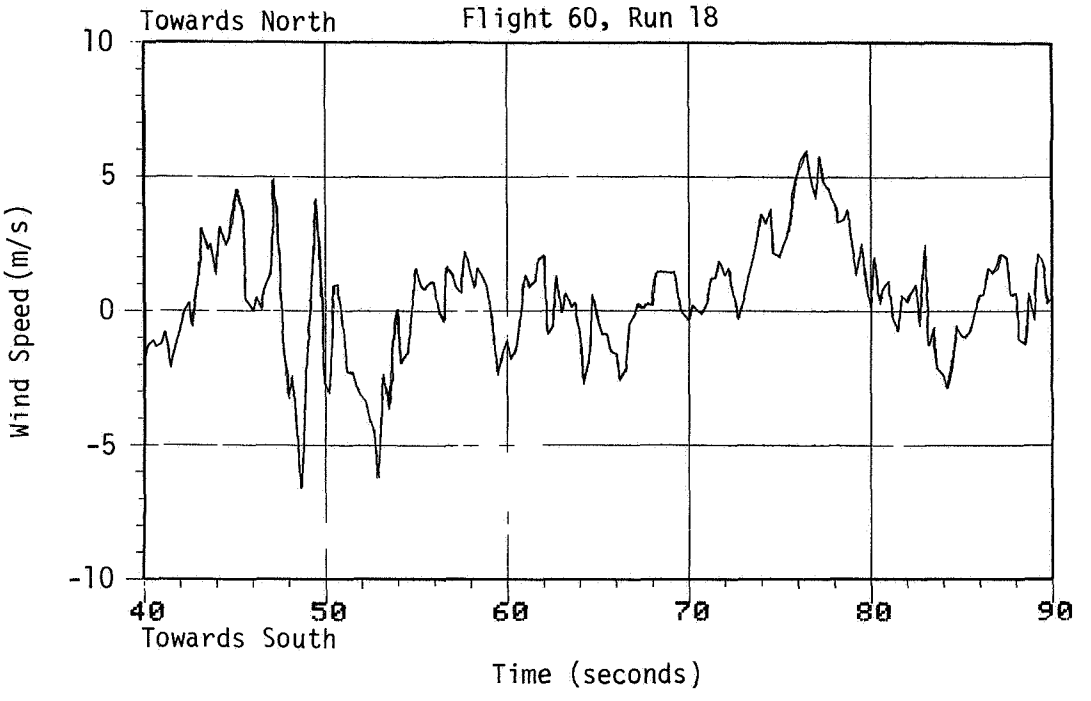

Figure 4.4. Longitudinal wind component (north/south).

illustrates the effect of adding the spanwise turbulence terms into the 6DOF flight simulation. With spanwise turbulence included, the amplitude of the oscillations generally increase and furthermore closer resemble the real flight.

Figure 4.7 shows the influence of the spanwise turbulence terms on the roll response of the 6DOF computer simulation. A noticeable increase in roll angle amplitude occurs at the 79- and 85-second marks as a result of the spanwise turbulence. Throughout the 50-second simulation, the spanwise turbulence excites the higher frequency roll response.

Figures 4.8 and 4.9 are generated from the 6DOF computer simulation. Total roll moment coefficient is given by expressing Equation 4.4 in coefficient form. Similarly, total yaw moment coefficient is obtained from the coefficient form of Equation 4.6. Again, the difference between the

solid and the dashed lines in Figures 4.8 and 4.9 is simply the addition of the spanwise turbulence terms of Equations 1.1 through 1.4 into the force and moment equations. The increase in high-frequency content of Figure 4.8 is due to the L_{ADD} term plotted in Figure 3.10. Much of the high-frequency is damped out as is evident in Figure 4.7, but the spanwise turbulence also contains lower frequencies which affect the roll response substantially. In Figure 4.9 the yaw moment coefficient seems to be far less affected by the addition of spanwise turbulence terms. This is to be expected since Figure 4.6 shows less influence from spanwise turbulence. Analyzing the relative influence of the terms in Equation 4.6, it is found that the rudder term is responsible for the characteristic shape of the yaw coefficient.

Thus, from the results presented in this chapter, it is demonstrated that spanwise turbulence affects the response of the aircraft. The roll mode is especially sensitive to variations in turbulence along the wing.

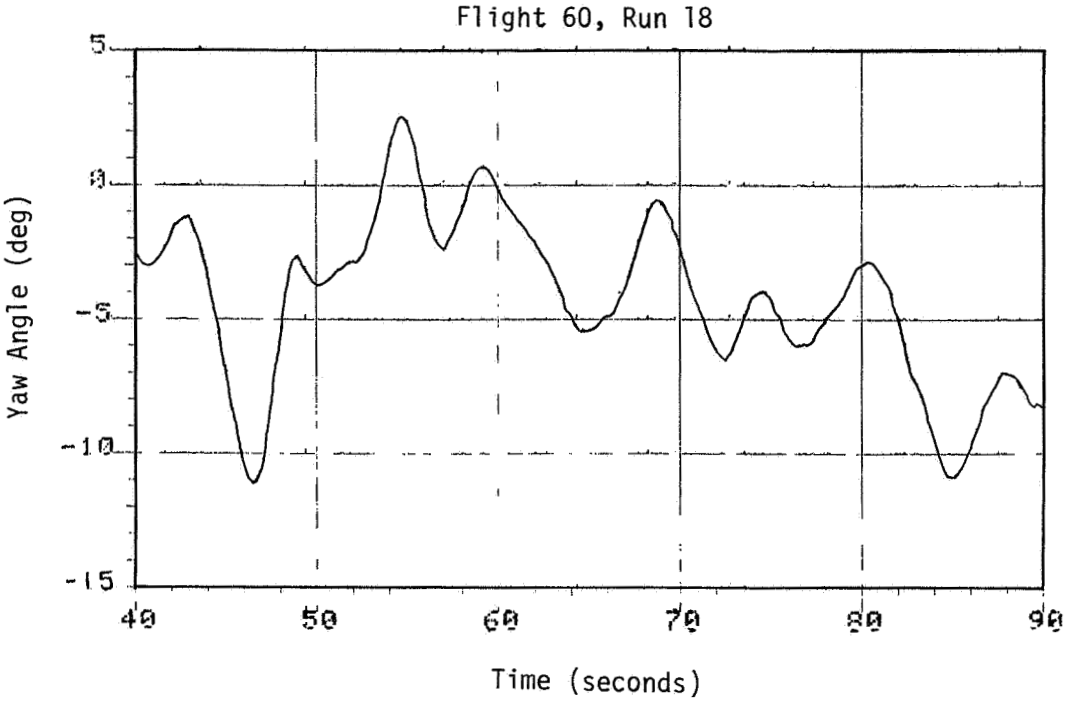

Figure 4.5. Recorded yaw angle.

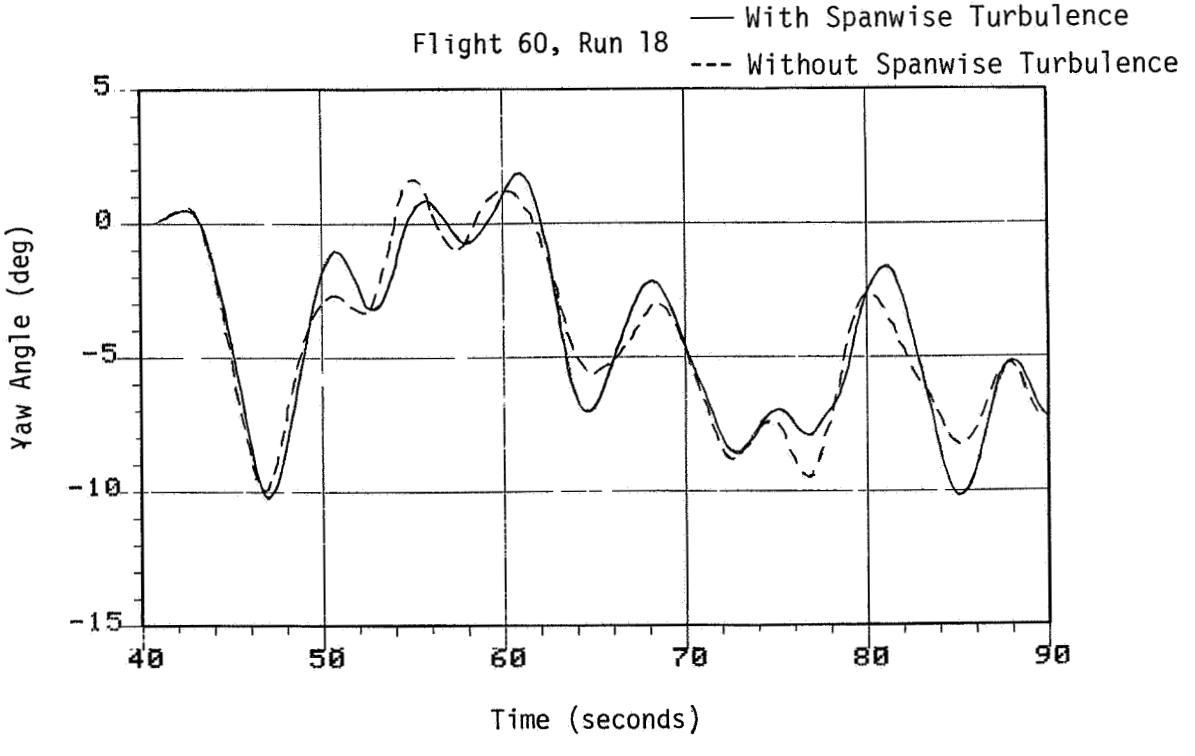

Figure 4.6. Calculated yaw angle.

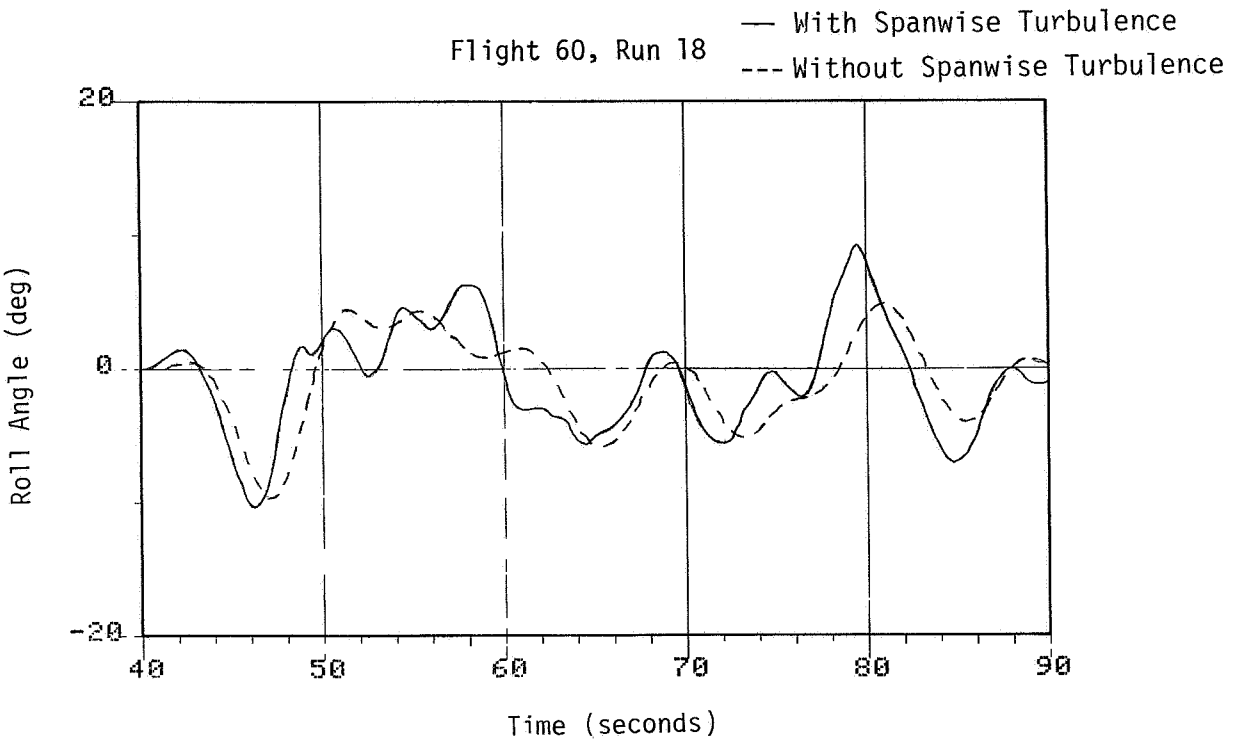

Figure 4.7. Calculated roll angle.

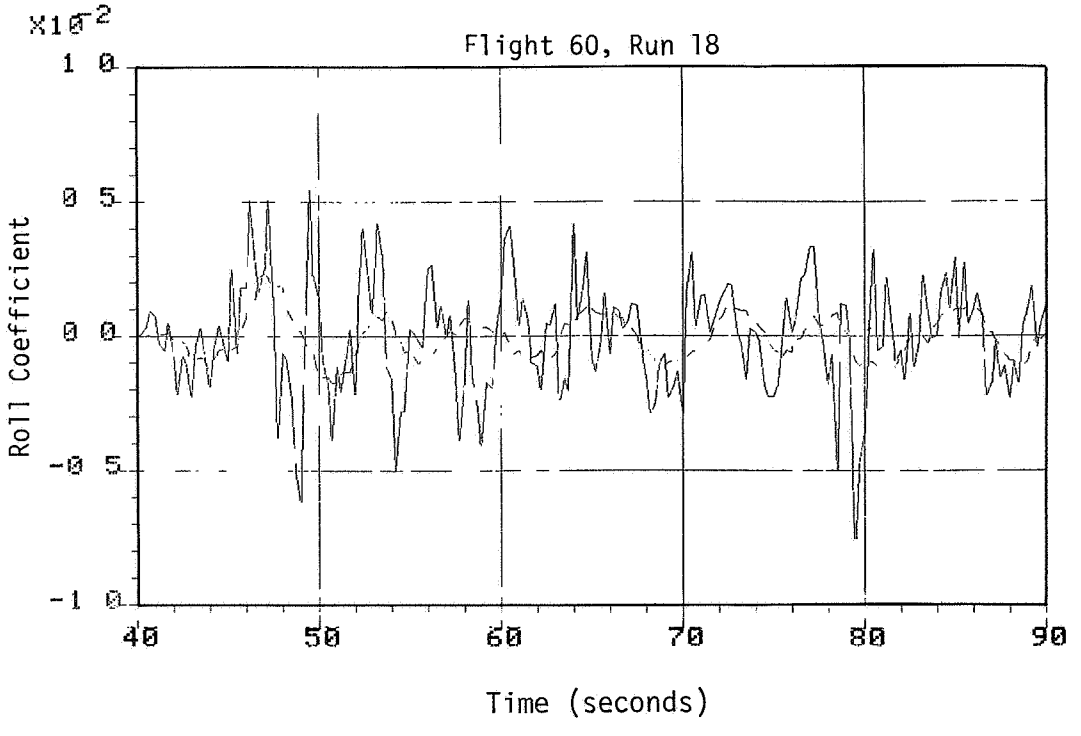

Figure 4.8. Calculated total roll moment coefficient.

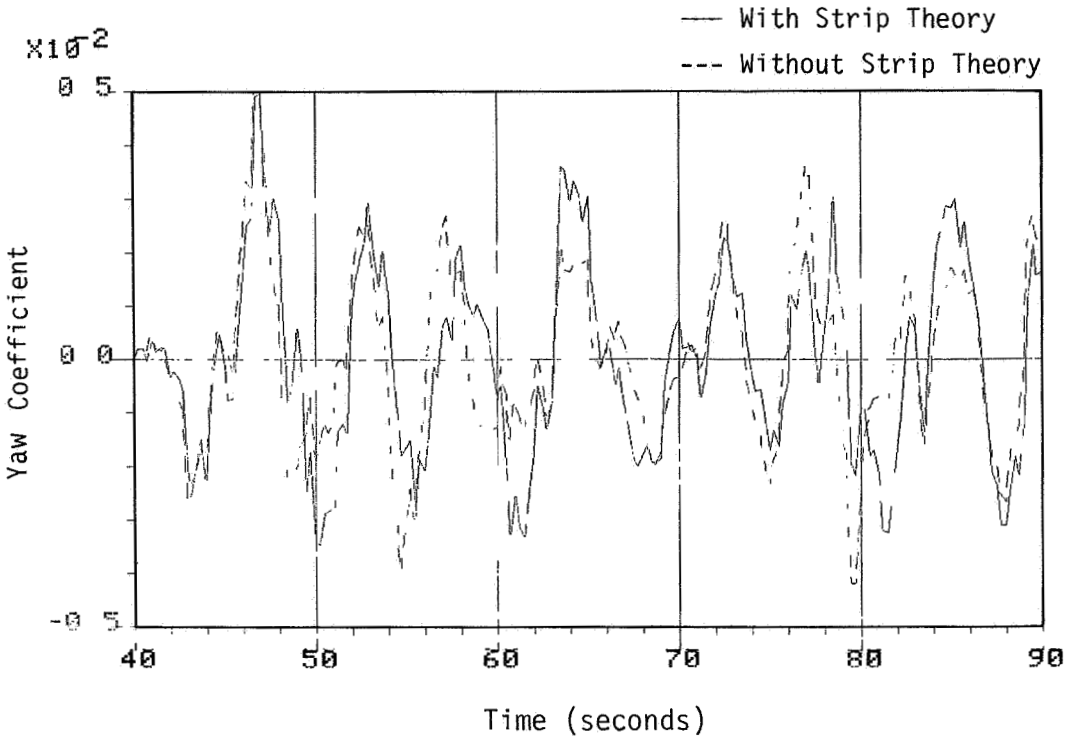

Figure 4 9. Calculated total yaw moment coefficient.

CHAPTER V

CONCLUSIONS

The results of this study are based on NASA B-57 flight test data. The magnitude of spanwise turbulence effects is quantified and also the influence of spanwise turbulence on airplane dynamic behavior is demonstrated. The severity of the turbulence recorded on the computer simulated test flight, Flight 60, Run 18, is best described by the 2.8 m/s standard deviation of the vertical gust component.

It is evident from the results that wind variations across the B-57 wing can indeed produce large aerodynamic moments on its wings. Such roll moments are equivalent of up to 10 degrees of aileron input. The influence of spanwise turbulence on the calculated roll mode is significant. The pilot workload is also increased.

The spanwise turbulence also affects the yaw mode of the aircraft as is illustrated by the calculations in this study. Since yaw moments produced by spanwise turbulence only represent a fraction of similar roll moments, the yaw mode is excited, but less severly than the roll mode.

The calculations of aerodynamic forces on the wing showed only small changes when spanwise turbulence was replaced by the traditional uniform distribution. The greatest difference in lift calculated due to spanwise turbulence is 10 percent of the aircraft weight, but generally the difference is closer to 2 percent.

The strip theory lift calculations were expressed as a lift-to-weight ratio and compared with the flight data load factor. With the

gust alleviation factor (see Appendix A) applied to the calculated loading, the difference between the two curves is negligible (Figure 3.5, page 24). The contribution to lift from aircraft dynamics is ignored in the theoretical calculations. This comparison suggests the strip theory lift calculations are realistic.

The six-degrees-of-freedom flight simulation is limited by a number of necessary assumptions. The aerodynamic modeling of the B-57, in particular, is critical. The aerodynamic coefficients and derivatives were estimated without any wind tunnel or test flight information. With these assumptions made, spanwise turbulence effects are shown to substantially influence response.

BIBLIOGRAPHY

BIBLIOGRAPHY

Babister, A. W. (1980). Aircraft Dynamic Stability and Response. New York: Pergamon Press, Inc.

Bisplinghoff, R. L. G. Isakson, and T. F. O'Brien (1951). "Gust Load on Rigid Aircraft with Pitching Neglected," Journal of Aeronautical Sciences, 13(33):33-39, January.

Camp, D. W., W. Campbell, W. Frost, H. Murrow, and W. Painter (1984). "NASA's B-57B Gust Gradient Program," Journal of Aircraft, 21(3): 175-182, March.

Campbell, W., D. W. Camp, and W. Frost (1983). "An Analysis of Spanwise Gust Gradient Data," Preprints: 9th Conference on Aerospace and Aeronautical Meteorology, p. 7, June 6-9, Omaha, Nebraska.

Coupry, Gabriel (1972). "Effect of Spanwise Gust Velocity of Airplane Response to Turbulence," Journal of Aircraft, 9(8):569-574, August.

Diederich, Franklin W., and J. A. Drischler (1957). "Effect of Spanwise Variations in Gust Intensity on the Lift Due to Atmospheric Turbulence," NACA TN 3920.

Etkin, B. (1972). Dynamics of Atmospheric Flight. New York: John Wiley and Sons, Inc.

Eichenbaum, Fredrick (1971). "A General Theory of Aircraft Response to Three-Dimensional Turbulence," Journal of Aircraft, 8(5):353-360, May.

Frost, W., and R. L. Bowles (1984). "Wind Shear Terms in Equations of Aircraft Motion," Journal of Aircraft, 21(11):866-872, November.

Frost, W., H. P. Chang, K. L. Elmore, and J. McCarthy (1984). "Simulated Flight Through JAWS Wind Shear," Journal of Aircraft, 21(10):797-802, October.

Frost, W., and M. C. Lin (1983). "Statistical Analysis of Turbulence Data from the NASA Marshall Space Flight Center Atmospheric Boundary Layer Tower Array Facility," NASA CR 3737.

Fuller, J. R. (1968). "Procedure for Evaluating the Spacewise Variations of Continuous Turbulence of Airplane Responses," Journal of Aircraft, 5(1):49-52, January-February.

Kuethe, A. M., and C. Y. Chow (1976). Foundations of Aerodynamics. New York: John Wiley and Sons, Inc.

Houbolt, John C., R. Steiner, and K. G. Pratt (1964). "Dynamic Response of Airplanes to Atmospheric Turbulence Including Flight Data on Input and Responses," NASA TR R-199.

Painter, W. D. and D. W. Camp (1983). "NASA B-57B Severe Storms Flight Program," NASA TM-84921.

APPENDICES

APPENDIX A

GUST ALLEVIATION FACTOR

The strip theory calculations of lift in Chapter III are based on an instantaneous angle of attack in a steady-state condition. While this is approximately true for a gradually applied disturbance, it overestimates the loads for a sudden disturbance such as that due to a sharp-edged gust. The change of lift is gradual (transient) until steady-state value is reached. The response depends upon the characteristics of the gust as well as the aircraft.

For a gradual upgust as illustrated in Figure A.1, the normal acceleration response will be as shown in Figure A.2 (Babister 1980). The time (t_1) it takes the airplane to fly through the transition (s_1) is related to the airspeed V as follows:

$$s_1 = Vt_1 \tag{A.1}$$

The vertical acceleration increases almost linearly up to time t_1 and then falls off exponentially. The gust alleviation factor K is defined (Babister 1980, p. 108) as the ratio of the maximum vertical acceleration experienced due to a given gust to the theoretical maximum vertical acceleration in a sharp-edged gust with steady-state conditions. As expected, the gust alleviation factor decreases as the transition region increases. Assuming steady-state conditions, the gust factor becomes unity as s_1 goes to zero. Furthermore, as the transition region becomes large, the unsteady flow effects get smaller. Figure A.3 which represent a plot of the factor K reproduced from Bisplinghoff (1951). Variable H is the normalized gust transition region defined as:

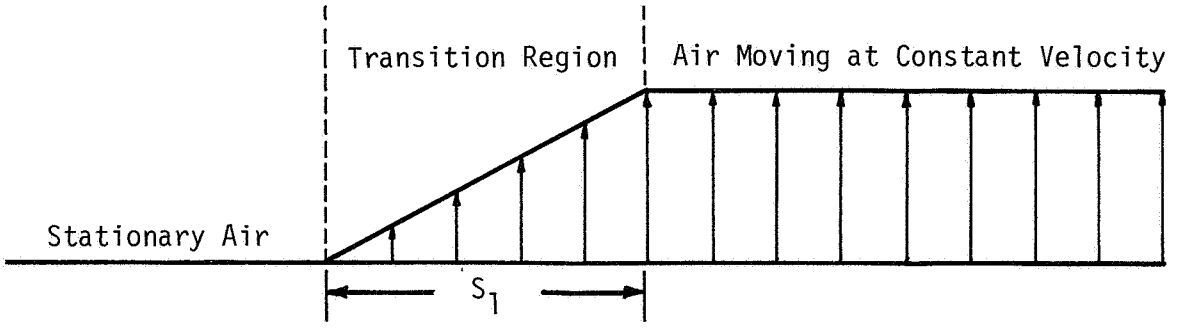

Figure A.1. A gradual gust.

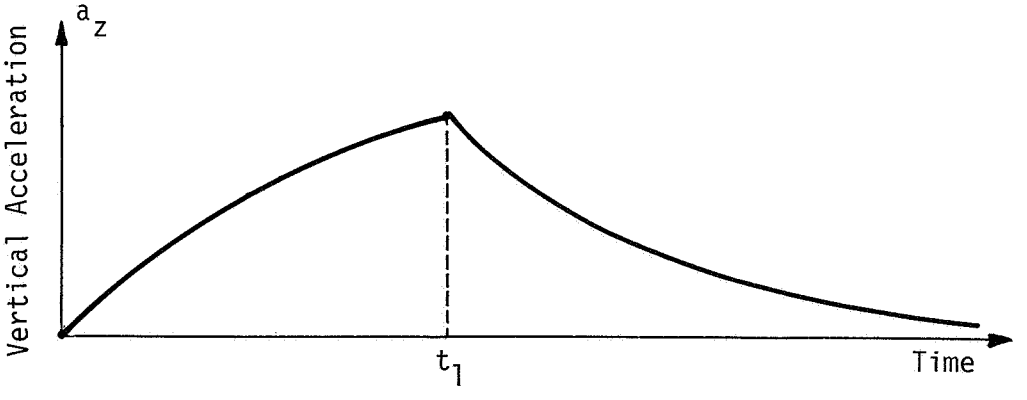

Figure A.2. Vertical acceleration due to a gradual gust.

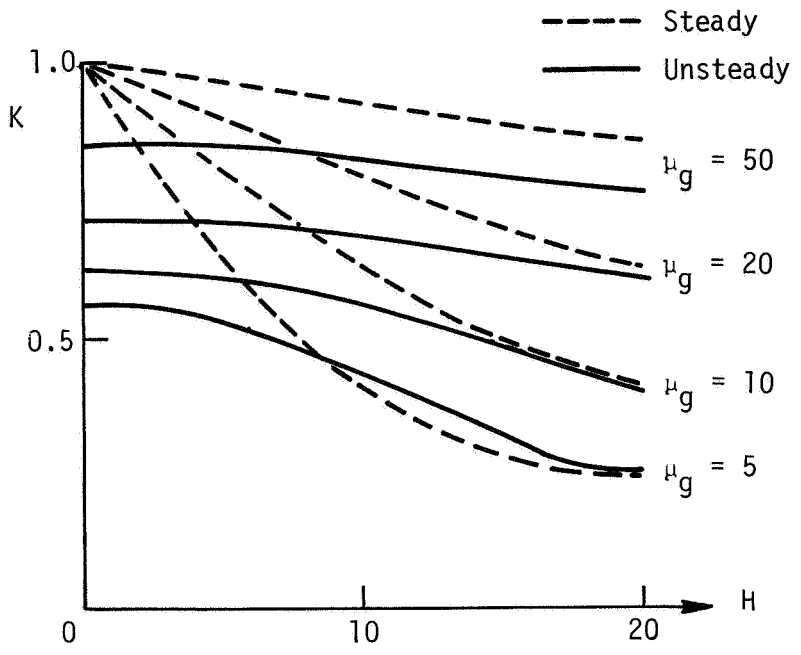

Figure A.3. Gust alleviation factor.

$$H = s_1/\bar{c} \tag{A.2}$$

and μ_g is a mass parameter given by:

$$\mu_g = \frac{m}{\frac{1}{2}\rho S a_\infty \bar{c}} \tag{A.3}$$

The plot illustrates the importance of the unsteady effects for sharp-edged gusts.

The mass parameter indicates that for an aircraft of low mass, the alleviation factor or acceleration ratio gets small as the transition region increases. For a high mass aircraft, the acceleration ratio is less dependent upon the length of the transition region. However, the maximum acceleration itself is inversely proportional to the mass parameter and is given by:

$$a_{z_{max}} = \frac{V\omega_z}{\mu_g \bar{c}} \qquad (A.4)$$

where ω_z is the maximum vertical gust velocity.

For the B-57, the following values are obtained under the flight conditions in question:

$\mu_g = 24.6$

$H = 10.6$

$K = 0.7$

This value for the gust gradient coefficient is applied to the lift calculations in the following way. The difference between lift and weight is computed at each time step, and this difference is multiplied with K. That fraction is added back to the weight to give the corrected lift. The procedure is illustrated in Figure A.4 for a lift curve which is artificially constructed.

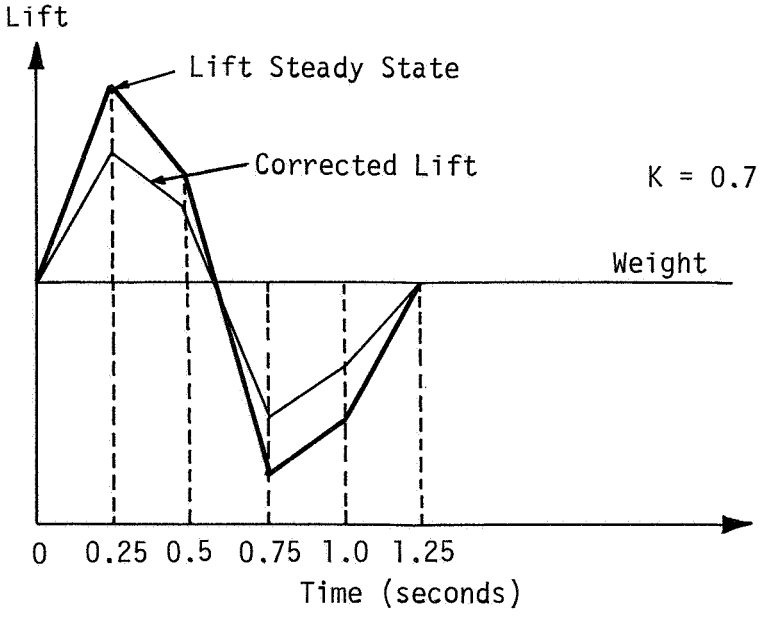

Figure A.4. Correction to lift using the gust alleviation factor K.

APPENDIX B

B-57 CHARACTERISTICS USED IN SIMULATION OF FLIGHT 60, RUN 18

1. TRIM CONDITIONS FOR FLIGHT 60, RUN 18

Trim airspeed	v = 113.0 m/s (370.7 ft/sec)
Air density	ρ = 0.96186 kg/m^3 (0.00187 slugs/ft^3)
Tail incidence angle	i_t = -0.22 degrees
Thrust force	T = 36,509 Newtons (8,207 lbf)
Aircraft mass	W = 20,420 kg (45,017 lb)
Level flight, no flaps, gear up	

2. AIRPLANE PARAMETERS

Wing area	S = 89.2 m^2 (960 ft^2)
Wing span	b = 19.5 m (63.95 ft)
Mean aerodynamic chord	c_{mac} = 4.57 m (15 ft)
Aspect ratio	AR = 4.3
Moments of inertia	I_{xx} = 325,300 kg - m^2 (240,000 slug ft^2)
	I_{yy} = 271,100 kg - m^2 (200,000 slug ft^2)
	I_{zz} = 650,600 kg - m^2 (480,000 slug ft^2)
	I_{zx} = 11,000 kg - m^2 (8,100 slug ft^2)

3. AERODYNAMIC COEFFICIENTS AND STABILITY DERIVATIVES

$C_{L_o} = 0.07$

$C_{L_\alpha} = 4.98/\text{rad}$

$C_{L_{\delta_e}} = 0.419/\text{rad}$

$C_{L_{i_t}} = 0.670/\text{rad}$

$C_{L_q} = 2.90/\text{rad}$

$C_{L_{\dot{\alpha}}} = 1.45/\text{rad}$

$C_{D_o} = C_L^2/13.5$

$C_{m_o} = 0.064$

$C_{m_\alpha} = -1.0/\text{rad}$

$C_{m_{\delta_e}} = -0.860/\text{rad}$

$C_{m_{i_t}} = -1.72/\text{rad}$

$C_{m_q} = -9.65/\text{rad}$

$C_{m_{\dot{\alpha}}} = -5.83/\text{rad}$

$C_{y_\beta} = -0.286/\text{rad}$

$C_{y_{\delta_r}} = -0.071/\text{rad}$

$C_{n_\beta} = 0.0573/\text{rad}$

$C_{n_{\delta_r}} = -0.0321/\text{rad}$

$C_{n_{\delta_a}} = -0.00286/\text{rad}$

$C_{n_p} = -0.070/\text{rad}$

$C_{n_r} = -0.200/\text{rad}$

$C_{\ell_\beta} = -0.0286/\text{rad}$

$C_{\ell_{\delta_r}} = 0.0040/\text{rad}$

$C_{\ell_{\delta_a}} = 0.0458/\text{rad}$

$C_{\ell_p} = -0.5/\text{rad}$

$C_{\ell_r} = 0.081/\text{rad}$

APPENDIX C

CONTROL LAWS

The six-degrees-of-freedom simulation uses the following automatic control laws:

$$\delta_e = DE1(V_z - V_{e_{ref}}) + DE2(\theta - \theta_{trim}) \quad (C.1)$$

$$\delta_a = DA1(V_y - V_{a_{ref}}) + DA2 \cdot \phi \quad (C.2)$$

$$\delta_r = DR1(V_y - V_{r_{ref}}) + DR2 \cdot \psi \quad (C.3)$$

where:

DE1 = -0.0025 (Elevator control gain factor #1)

$V_{e_{ref}}$ = 2.0 m/s

DE2 = 0.06 (Elevator control gain factor #2)

θ_{trim} = 1.203 degrees

and

DA1 = -0.005 (Aileron control gain factor #1)

$V_{a_{ref}}$ = -0.08 V_y

DA2 = -0.80 (Aileron control gain factor #2)

and

DR1 = 0.015 (Rudder control gain factor #1)

$V_{r_{ref}}$ = -0.12 V_y

DR2 = 0.50 (Rudder control gain factor #2)

APPENDIX D

FLIGHT INFORMATION

1. Flight 6, Run 21

Date: July 14, 1982

Location: Denver, Colorado

Project: Joint Weather Airport Studies (JAWS)

Start time: 14:41:58 MDT

Duration: 41.5 seconds

Altitude above ground: 1000 feet

Mean airspeed: 96 m/s (315.0 ft/sec)

Flight description: Level flight

2. Flight 60, Run 18

Date: February 1, 1984

Location: Boulder, Colorado

Project: Orographic Effects Campaign

Start time: 16:57:15 MST

Duration: 140 seconds

Altitude above ground: 1500 feet

Mean airspeed: 113 m/s (370.7 ft/sec)

Flight description: Level flight

1 REPORT NO.	2 GOVERNMENT ACCESSION NO.	3 RECIPIENT'S CATALOG NO.
NASA CR-3961		

4 TITLE AND SUBTITLE	5 REPORT DATE
Analysis of Aerodynamic Coefficients Using Gust Gradient Data. Spanwise Turbulence Effects on Airplane Response	February 1986
	6 PERFORMING ORGANIZATION CODE
7 AUTHOR(S)	8 PERFORMING ORGANIZATION REPORT #
Erik A. Ringnes and Walter Frost	
9 PERFORMING ORGANIZATION NAME AND ADDRESS	10 WORK UNIT NO.
FWG Associates, Inc. Route 2, Box 271-A Tullahoma, TN 37388	M- 512
	11 CONTRACT OR GRANT NO. NAS8-35186
	13 TYPE OF REPORT & PERIOD COVERED
12 SPONSORING AGENCY NAME AND ADDRESS	Contractor Report June 3, 1983--June 2, 1985
National Aeronautics and Space Administration Washington, D.C. 20546	14 SPONSORING AGENCY CODE

15 SUPPLEMENTARY NOTES

Technical Monitor Margaret B. Alexander Prepared for the Atmospheric Sciences Division, Systems Dynamics Laboratory, Marshall Space Flight Center, Alabama, 35812

16. ABSTRACT

The purpose of this study was to determine the influence of spanwise turbulence on airplane dynamic behavior. Calculations are based on data collected from test flights with the NASA B-57 research aircraft. The approach taken is to first compute aerodynamic forces and moments due to a spanwise distribution of angle of attack and airspeed. Secondly, these quantities are incorporated into the equations of motion. Simulation of flights done with the effects of spanwise turbulence included are compared to simulations without any spanwise turbulence. The findings of the study are that the moments developed by turbulence along the span are significant and that more realistic flight simulation can be achieved by including the spanwise turbulence terms.

17 KEY WORDS	18. DISTRIBUTION STATEMENT
Spanwise Turbulence Aerodynamic Forces and Moments Aviation Safety Flight Simulation	Unclassified--Unlimited STAR Category 47

19 SECURITY CLASSIF. (of this report)	20. SECURITY CLASSIF. (of this page)	21 NO. OF PAGES	22. PRICE
Unclassified	Unclassified	68	A04

For sale by National Technical Information Service, Springfield, Virginia 221

NASA-Langley, 1